www.sciencemag.org/cgi/content/full/science.aah7111/DC1

Supplementary Materials for

CRISPRi-based genome-scale identification of functional long noncoding RNA loci in human cells

S. John Liu,* Max A. Horlbeck,* Seung Woo Cho, Harjus S. Birk, Martina Malatesta, Daniel He, Frank J. Attenello, Jacqueline E. Villalta, Min Y. Cho, Yuwen Chen, Mohammad A. Mandegar, Michael P. Olvera, Luke A. Gilbert, Bruce R. Conklin, Howard Y. Chang, Jonathan S. Weissman,†‡ Daniel A. Lim†‡

*These authors contributed equally to this work.
†These authors contributed equally to this work.
‡Corresponding author. Email: daniel.lim@ucsf.edu (D.A.L.); jonathan.weissman@ucsf.edu (J.S.W.)

Published 15 December 2016 on *Science* First Release
DOI: 10.1126/science.aah7111

This PDF file includes:

Other supplementary material for this manuscript includes:

Tables S1 to S11 (Excel format)

Materials and Methods

lncRNA CRISPRi library design

lncRNA target selection

LncRNA annotations were retrieved from Ensembl build 75 (using the biotypes lincRNA, antisense, 3 prime overlapping ncRNA, processed transcript, sense intronic, sense overlapping) (*39*), the Broad human lincRNA catalog (*37*), the MiTranscriptome (*38*) , and a set of human brain specific lncRNAs (*42*). Annotations were merged using the cuffmerge command in Cufflinks v2.2.1 (*62*).

LncRNAs that were transcribed in at least one of the 7 cell lines in this study were identified by quantifying the expression of lncRNAs using RNA-seq data. RNA-seq data were obtained from ENCODE and other sources: HEK293T (GSE56010), HeLa (GSE30567, GSE33480, GSE23316), K562 (GSE30567, GSE33480, GSE23316), MCF7 (GSE30567, GSE33480), MDAMB231 (GSE73526, GSE45732), iPS (clone PCBC15hsi2012040401 (*63*)), HFF (GSE69906). RNA-seq was performed in-house for U87 cells, using the illumina TruSeq Stranded mRNA kit. Reads were quality trimmed using seqtk v1.0 and aligned to the human genome (GRCh37) with tophat v2.0.10, using the merged transcriptome reference as the transcriptome index, the prefilter-multihits flag, and strand specific flag when appropriate. Transcript abundance estimation was performed using Cufflinks v2.2.1. For each gene, the median FPKM value of the replicate samples were obtained. For each cell line, a minimum expression threshold was set between 0.25-0.50 FPKM in order to screen as many genes as possible, given cell culture scale limitations. 21,578 lncRNAs were identified.

Generating lncRNA TSS annotations

From these 21,578 transcripts passing the expression filter, an initial set of 17,740 TSSs were obtained from transcripts belonging to the same gene and with 5' ends within 100bp of each other. These TSS annotations were further refined using the FANTOM cap analysis of gene expression (CAGE)-based TSS annotations as previously described (*35*) with adjustments. LncRNA TSS annotations could not be directly matched to FANTOM "p1@gene" CAGE peaks, and instead were matched to any same-stranded CAGE peak within 400bp labeled as "p1" or "p2," and annotation support was labeled as "CAGE, primary peaks." If no primary peaks were found, annotations could instead be refined by robust or permissive peaks within 200bp of the starting annotation, and were labeled as "CAGE, robust peak" or "CAGE, permissive peak," respectively. Where no CAGE peaks were found (due to the cell type-specific nature of lncRNA expression only 30% of TSS annotations were refined with CAGE peaks), the TSS as determined by the annotation sets above was used and labeled "Annotation." 66 of the original TSSs were assigned the same start site by this method, reducing the total number targeted to 17,674. This annotation is included as Table S1. As detailed below, a further 692 TSSs could not be uniquely targeted, reducing the total TSSs to 16,982. Finally, to avoid redundant information from different TSSs located in close proximity, TSSs within 100bp of each other were assigned to a single gene ID (designated LHnnn in Tables S1-6,8) for a total of 16,401 distinct lncRNA target loci.

sgRNA selection

All potential sgRNAs within 25bp upstream and 500bp downstream of the refined lncRNA TSS annotations were scored for predicted activity using the hCRISPRi-v2.1 algorithm, scored for off-target sites near TSSs and in the genome using weighted Bowtie v1.0.0 (*64*), and filtered for required restriction sites (BstXI, BlpI, and SbfI) and overlap with higher-ranking sgRNAs as previously described (*35*). For 692 TSSs, 10 sgRNAs passing all filters could not be found and were discarded. 87.5% of sgRNAs accepted into the library passed the highest off-target stringency threshold, while 10.9% passed at the second-highest stringency. Non-targeting control sgRNAs were generated randomly weighted by the per-base nucleotide frequencies of the targeting sgRNAs in the library, and filtered for no target sites in the genome. sgRNAs targeting lncRNA genes specifically expressed in a subset of cell types were assigned to the appropriate hierarchical sublibrary (along with a proportional number of non-targeting controls) to enable screening only the desired gene sets (Figure S2A). Sublibraries were designed as the intersection of genes expressed in the cell lines indicated in Figure S2A, and then the full set of genes for a given cell line could be generated by combining sublibraries as follows:

iPSC = Common + (iPSC, HFF) + iPSC
HFF (not screened in this study) = Common + (iPSC, HFF) + iPSC
U87 = Common + Cancer common + (U87, HEK293T) + U87
HEK293T = Common + Cancer common + (U87, HEK293T) + HEK293T
K562* = Common + Cancer common + (K562, HeLa, MCF7) + (K562, HeLa) + K562
HeLa = Common + Cancer common + (K562, HeLa, MCF7) + (K562, HeLa) + HeLa
MCF7/MDA-MB-231 = Common + Cancer common + (K562, HeLa, MCF7) + MCF7
*all 13 sublibraries were screened in K562s to validate the cell line expression sublibrary strategy; see Figure 5C

Oligonucleotide pools were designed with flanking cloning and PCR sites as described, synthesized by Agilent Technologies (Santa Clara, CA), and cloned into the library sgRNA expression vector pCRISPRia-v2 (*23, 35*).

For the *PVT1* tiling library, all possible sgRNAs from 25bp upstream of the *PVT1* locus to 25bp downstream that passed the second-highest off-target stringency filter and restriction site filters were included. Non-targeting sgRNAs matching this design in base composition and off-target stringency were included, and oligonucleotide pools were synthesized and cloned as above.

CRISPRi screens

Growth screens

Several cell lines expressing dCas9-KRAB were obtained from previous publications: HEK293T(*22*), HeLa(*22*), K562 (*23*), iPSCs (WTC-CRISPRi Gen IC)(*33*), and U87(*42*). MCF7 and MDA-MB-231 were generated for this study by infecting lentivirus expressing dCas9-KRAB-BFP (Addgene #46911; (*22*)) and sorting for single cell clones stably expressing high BFP. Replicates for these cell lines were performed in different clones. All cell lines except iPSCs were infected in duplicate with sgRNA the sublibraries described above or the *PVT1* tiling library, packaged with TransIT-LT1 (Mirus, Madison,

WI) transfection in HEK293T cells (not expressing dCas9-KRAB), at an initial infection rate of 30-50% (300-500x coverage of the library). Cells were cultured for two days following infection, treated for two days with 0.75-1.00 μg/mL puromycin, allowed to recover for one day, and then cultured at a minimum coverage of 1000x for 12 days (K562, HEK293T, U87, HeLa) or 20 days (MCF7, MDA-MB-231) starting from this "T0." K562 cells were passaged daily, while adherent cells were split on alternate days. iPSCs were infected at ~15% infection (with double the starting cell population to yield 300x coverage), grown for 3 days, selected with 1.5 μg/mL puromycin for 9 days, and allowed to recover for 3 days. iPSCs were then divided into two independent replicates and treated daily with 2μM doxycycline starting from this T0 and for the following 18 days (with primary endpoint at 12 days used here unless otherwise specified). Cells with a minimum of 1000x library coverage were harvested the day following puromycin recovery (T0) and at the endpoint, and processed for sequencing on Illumina HiSeq 2500 or 4000 as previously described(*23, 35*).

Sequencing reads were aligned to the expected CRiNCL library sequences, counted, and quantified using the ScreenProcessing pipeline (https://github.com/mhorlbeck/ScreenProcessing; (*35*)) Negative control genes were generated by randomly sampling (with replacement) ~10 non-targeting sgRNAs per negative control gene to match the true gene TSSs targeted by the library, and then scoring the negative control genes for effect size and Mann-Whitney p-value as was done for the true genes. Genes (LHnnn) with multiple TSSs were collapsed to a single score by selecting the one with the lowest Mann-Whitney p-value.

In order to call hit genes from screens, we defined a "screen score" incorporating both the effect size and the p-values of genes in each screen. The screen score was calculated as | γ z-score from negative control gene distribution | x $-\log_{10}$ p-value, and for all screens a threshold of greater than or equal to 7 was applied to call hits.

Neighbor hits were classified by first calculating the distance between the each lncRNA TSS and the TSS of the closest protein coding gene (TSS-pc distance). LncRNAs whose TSS-pc distance was less than 1000 bp, and whose neighboring protein coding gene was 1) scored as essential in our previous screen in K562 cells (*23*), 2) expressed in the cell type in consideration, and 3) had the same phenotype direction as the lncRNA, were then classified as neighbor hits. Hits that did not meet these criteria were left as lncRNA hits.

OCT4 FACS-based screen

iPSCs were harvested 9 days post-doxycycline addition from the growth screen samples above and fixed with 4% paraformaldehyde for 10 minutes at room temperature followed by PBS wash. 9 days was chosen to balance the longer duration of continuous target gene knockdown with dropout of cells containing sgRNAs conferring a negative growth phenotype. Cells were permeablized with 0.5% saponin (Sigma) in PBS with 4% FBS and 2mM EDTA, stained with 1:100 mouse monoclonal α-*OCT3/4* antibody (sc-5279, Santa Cruz Biotechnology), washed with permeablization buffer, and stained with 1:200 Goat α-Mouse IgG-488 (A11029, Invitrogen) (*33*). Cells in the top and bottom 30% of *OCT4* signal as measured on the FITC-A channel were sorted for purity on a FACS

AriaII custom. Sorted cells were then harvested for de-crosslinked genomic DNA using QIAamp DNA Formalin Fixed Paraffin Embedded Tissue kit (QIAGEN) following manufacturer's instructions but omitting paraffin removal steps, using one column per million sorted cells. Genomic DNA was directly amplified for Illumina sequencing using Q5 DNA polymerase (New England Biolabs) and sequenced on a HiSeq 4000. Sequencing data was analyzed as described above.

A screen for protein-coding genes required for robust growth in iPSCs was performed as with the iPSC lncRNA screen, with an endpoint at 14 days post-doxycycline addition. The screen was performed using the hCRISPRi-v2 H1 Drug Targets, Kinases, and Phosphatases sublibrary with 5 sgRNAs/gene (*35*), and was analyzed as above.

sgRNA Validation

sgRNAs for individual validation were cloned by annealing oligo pairs containing the sgRNA protospacer and flanking BstXI and BlpI cloning sites and ligating the resulting fragment into the sgRNA expression vector pU6-sgRNA EF1Alpha-puro-T2A-BFP (Addgene #60955). Internally controlled growth assays were performed by infecting cells with sgRNA lentiviruses at MOI < 1.0 and measuring the sgRNA+ fraction by BFP using flow cytometry on an LSRII (BD). Experiments were performed in biological triplicates from the infection step.

RT-qPCR

Cells were puromycin selected for 4 d (1 μg/mL) and subjected to 1 d recovery. K562 cells were infected for 48 hr, followed by 2 d puromycin treatment (3 μg/mL) and 2 d recovery. RNA was harvested with TRIzol and purified using the Direct-zol MiniPrep RNA purification kits (Zymo Research) with the on-column DNAse digestion step. cDNA were prepared with Transcriptor First Strand cDNA Synthesis Kit (Roche) using the oligo-dT protocol, and RT-qPCR was performed using LightCycler 480 SYBR Green I Master Mix (Roche) on a LightCycler 480 instrument (Roche). Experiments were performed in biological triplicates from the infection step. sgRNA protospacer sequences and RT-qPCR primers are listed in Table S11.

RNA-seq sample preparation and data analysis following CRISPRi

Cells were infected with sgRNA lentiviruses for 48 hr, followed by 4 d puromycin treatment (1 μg/mL) and 1 d recovery. K562 cells were infected for 48 hr, followed by 2 d puromycin treatment (3 μg/mL) and 2 d recovery. RNA was harvested using TRIzol and purified using the Direct-zol MiniPrep RNA purification kits (Zymo Research) with the on-column DNAse digestion step. RNA integrity was confirmed using the Agilent 2200 RNA ScreenTape. RNA-seq libraries were generated using TruSeq HT Stranded mRNA kit according to manufacturer's protocol (illumina). cDNA was validated using the Agilent 2200 DNA 1000 ScreenTape, Qubit 2.0 Fluorometer (Life Technologies), and ddPCR (Bio-Rad). Cluster generation and sequencing was performed on a HiSeq 4000, using the single end 50 read protocol. Reads were aligned to the human genome (GRCh37) using the spliced read aligner HISAT2 v2.0.3 (*65*) against an index containing SNP and transcript information (*genome_snp_tran*). Quantification of Ensembl build 75 genes was carried out with featureCounts (*66*) using only uniquely mapped reads.

Library complexity was calculated by counting the number of genes with greater than 2 reads, and knockdown efficiency was calculated by normalizing gene Transcripts per Million (TPM) for the experimental samples with the mean TPM of the control knockdown samples. Samples with fewer than 11,000 genes detected and weaker than 40% lncRNA knockdown were filtered. Pairwise Pearson correlations between RNA-seq samples were obtained using the sets of genes exhibiting significant variation within each cell type using the likelihood ratio test in DESeq2 (*67*) with an adjusted p value threshold of 0.001. Differential expression analysis for individual lncRNA knockdowns was performed using the Wald test in DESeq2 with an adjusted p value threshold of 0.05, using unique sgRNAs against the same lncRNA TSS as biological replicates. For hierarchical clustering of co-expressed genes across multiple samples, we first grouped cells by cell type and then by the direction of phenotype of the sgRNA. Within each subgroup, we obtained the set of variable genes using the likelihood ratio test in DESeq2 (*67*) with an adjusted p value threshold of 0.001. These genes were then used for complete linkage hierarchical clustering using Pearson correlation coefficients as the distance metric. Sequencing data are deposited in GSE85011.

ChIP-seq sample preparation and data analysis

Cells were infected with sgRNA lentiviruses for 48 hr, followed by 4 d puromycin treatment (1 ug/mL) and 1 d recovery. Genome-wide histone modifications were determined by ChIP against H3K9me3 (Abcam ab8898) on 5 million cells as described in (*68*). Cells were cross-linked by adding 37% formaldehyde to a final concentration of 1% into culture medium and gently shaking for 10 min at room temperature. Reaction was quenched with glycine, and cells were then washed twice with ice-cold PBS containing protease inhibitors (1mM PMSF, 1X Roche cOmplete EDTA-free cocktail). Cells were scraped off of the plate using a cell lifter and pelleted for 5 min at 2,000 rpm at 4°C. Pellet was snap-frozen in liquid nitrogen and stored at −80°C. Pellet was then thawed and resuspended in Cell Lysis Buffer (5 mM PIPES pH 8, 85 mM KCl, freshly added 1% IGEPAL) with protease inhibitors (Pierce Halt Protease Inhibitor Cocktail). Cells were then homogenized using a type B glass dounce homogenizer, pelleted, and resuspended in Nuclei Lysis Buffer (50 mM Tris-HCl pH 8, 10 mM EDTA, 1% SDS). Chromatin was sonicated in Diagenode TPX tubes using the Diagenode Bioruptor for 20 cycles and DNA was ranged from 150–700 bps as determined by gel electrophoresis. Debris was pelleted and discarded, and an aliquot was removed for Input DNA sequencing from the sonicated chromatin within the supernatant. Sonicated chromatin was then diluted 5-fold in IP Dilution Buffer (50 mM Tris–HCl pH 7.4, 150 mM NaCl, 1% IGEPAL, 0.25% deoxycholic acid, 1 mM EDTA pH 8) with protease inhibitors and pre-cleared with Life Technologies Protein G Dynabeads for 2 hr at 4°C. 5 µg of antibody was added per million cells, and samples were incubated overnight at 4°C. Antibody-bound chromatin was then collected using Life Technologies Protein G Dynabeads and washed twice with IP Dilution Buffer, twice with IP Wash Buffer 2 (100 mM Tris–HCl pH 9, 500 mM LiCl, 1% IGEPAL, 1% deoxycholic acid), and once with IP Wash Buffer 3 (100 mM Tris–HCl pH 9, 500 mM LiCl, 150 mM NaCl, 1% IGEPAL, 1% deoxycholic acid). Precipitated chromatin was then eluted for 30 min at 65°C with Elution Buffer (1% SDS, 50 mM $NaHCO_3$). ChIP and Input DNA crosslinks

were reversed by adding 5 M NaCl and heating at 65°C overnight. The following day, 10 mg/ml RNase A was added to precipitated chromatin, and chromatin was incubated for 30 min at 37°C. DNA was then recovered using Agencourt AMPure XP Beads and quantified using the Life Technologies Qubit Fluorometer.

ChIP DNA was then used for library preparation using the Kapa HyperPlus library preparation kit. 100ng of ChIP DNA was used for end repair and A-tailing. Illumina adapters were then ligated to the end-repair products. The library was amplified for 6 cycles before post-amplification cleanup using SPRI beads. Libraries were then quantified with the Life Technologies Qubit Fluorometer, and library size was confirmed using Agilent TapeStation 2200. ChIP-seq libraries were sequenced on a HiSeq 4000, 50 read single end.

Reads were aligned to the human genome (GRCh37) using bowtie v2.2.8 (*69*). Enrichment at promoter regions, which were defined as +/- 1kb of each TSS and generated from Ensembl GRCh37 build 75, were quantified using featureCounts v1.5.0-p2 (*66*). Signal was visualized using deepTools2 bamCoverage (*70*), normalizing reads to 1x sequencing depth. Differential H3K9me3 enrichment was analyzed using DESeq2 (*67*) , treating distinct sgRNAs against the same lncRNA TSS as replicate samples. Sequencing data are deposited in GSE85011.

Antisense oligonucleotide knockdown and proliferation assay

Antisense locked nucleic acid gapmers were designed against *LINC00263* using the Exiqon web server. Cells were transfected with the specified ASOs including negative control "A" at a final concentration of 50nM using Lipofectamine RNAimax Reagent (Invitrogen) according to the manufacturer's instructions. After 48 hours of transfection cells were seeded in duplicate. In order to maintain gene depletion, cells were transfected for a second time 7 days after the first transfection. Cell counting was performed every 2 days using Countess Automated Cell Counter (Invitrogen).

Flow cytometry for cell cycle analysis

Cells were transfected with the specified ASOs as described above. After 72 hours of transfection cells were pulsed with 33 μM bromodeoxyuridine (BrdU) for 20 min, and afterwards fixed in 70% ethanol. Subsequently cells were stained with primary anti-BrdU antibody (Clone B44; BD Biosciences) for 1 h, followed by 1 h incubation with Alexa Fluor 488 anti-mouse IgG (Invitrogen). DNA was counterstained by 0.1 mg/ml propidium iodide supplemented with RNase for 1 h at 37°C. Analysis was performed on a FACSCalibur using CellQuest software (BD). Quantification and analysis of cell-cycle profiles were obtained using FlowJo (Tree Star, Inc).

Machine learning of lncRNA properties

Genomic features were obtained from multiple sources. RNA-seq data were the same as used above for sgRNA library generation. Enhancer maps were obtained from the Fantom 5 Transcribed Enhancer Atlas (*48*), and VISTA Enhancer Browser set of experimentally confirmed human enhancers (*49*). Cell type-specific enhancer and super-enhancer maps for HeLa, U87, K562, and MCF7 cells were obtained from (*51*).

LncRNA loci were considered near a (super)enhancer if it overlapped with or was within 1kb of a mapped enhancer. Cancer associated SNPs from the NHGRI GWAS Catalog were obtained from (*50*) and noted if any were within 5 kb of a lncRNA locus. Cell type-specific copy number variation data for HEK293T, HeLa, K562, U87, and MCF7 cells were obtained from ENCODE (GSE40698) and intersected with lncRNA loci. ChIA-pet data for HeLa, K562, and MCF7 cell lines were obtained from ENCODE (GSE39495). LncRNA loci that were overlapped completely by a Pol2 or CTCF loop with a score of at least 400 were noted. LncRNAs with mouse orthologs were identified using Slncky (*52*).

To generate machine learning models, lncRNAs phenotypes were binarized as hit (1) or non-hit (0) and used as the response variable. Categorical variables were assigned as either 1 or 0. Missing data, e.g. super-enhancer or CNV information for cell lines for which data were not available, were assigned the value of 0. Predictor variables were then centered to the mean and z standardized. Expression levels were log transformed. To avoid confounding by nearby protein coding genes, only lncRNAs whose TSS were > 1kb from a protein coding TSS were considered. Several classes of models were generated and tested, using the R package caret on randomly sampled training (75% of data) and testing (25% of data) sets from our screen results. Logistic regression outperformed both support vector machines (least squares, polynomial kernel, radial kernel) and random forests in accurately classifying test sets of lncRNAs as hits or non-hit. Therefore, we used logistic regression to identify significant predictors of lncRNA hits. 100 iterations of ten-fold cross validation was performed by randomly withholding 10% of the dataset and training logistic regression models using the remaining data. Those predictors that repeatedly scored as significant ($p < 0.01$) were noted as reliable.

Author Contributions

M.A.H., S.J.L., J.S.W., D.A.L., and H.Y.C. conceived the project, interpreted the data, and wrote the manuscript. M.A.H. and S.J.L designed sgRNA library, performed RNA-seq, qPCR, growth assays, and analyzed data. S.J.L. performed screens in U87 and HeLa cells, 4C-seq, and machine learning. M.A.H. performed screens in K562, HEK293T, and iPS cells. S.W.C. performed screens and validation experiments in MCF7 and MDA-MB-231 cells. H.S.B., M.M., and F.J.A. performed qPCR, growth assays, and ASO experiments. D.H. performed ChIP-seq. J.E.V. cloned sgRNA libraries. M.Y.C. and Y.C. performed validation experiments. M.A.M., M.P.O., and B.R.C. contributed to iPSC experiments and performed iPSC protein-coding screens. L.A.G. contributed to data interpretation and project conception.

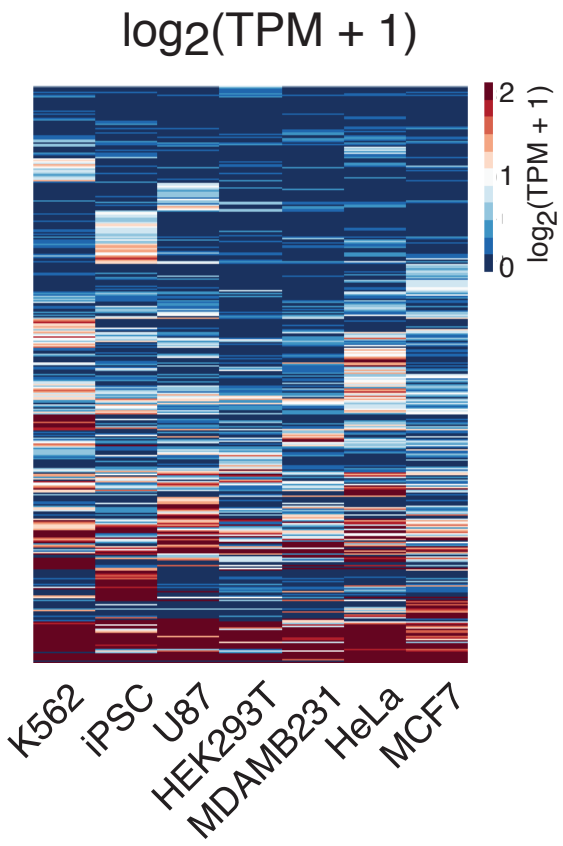

Figure S1. Expression levels of lncRNAs targeted in the CRiNCL library. Rows correspond to those used in Figure 1A. TPM, transcripts per million.

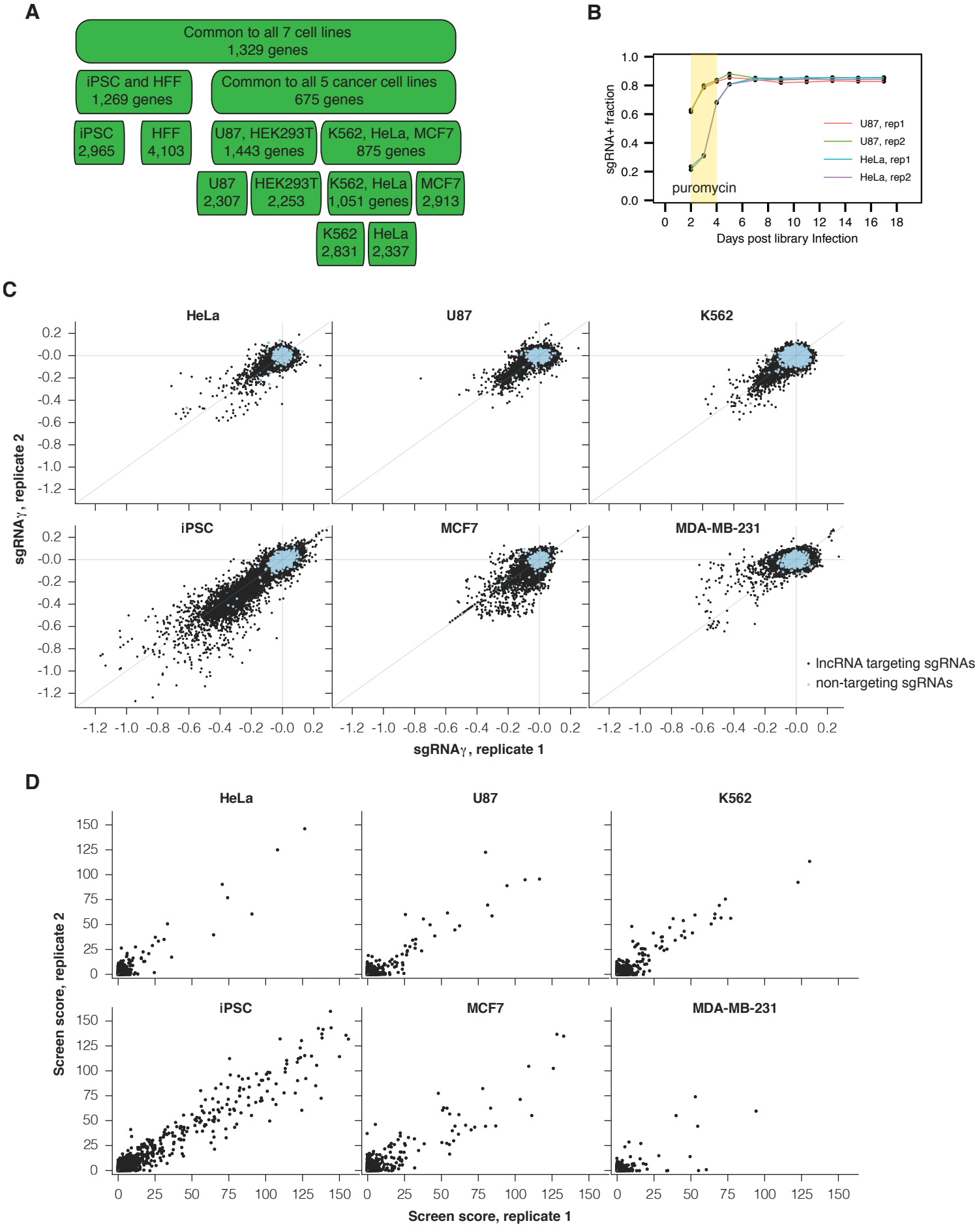
A
Common to all 7 cell lines
1,329 genes
iPSC and HFF
1,269 genes
Common to all 5 cancer cell lines
675 genes
iPSC
2,965
HFF
4,103
U87, HEK293T
1,443 genes
K562, HeLa, MCF7
875 genes
U87
2,307
HEK293T
2,253
K562, HeLa
1,051 genes
MCF7
2,913
K562
2,831
HeLa
2,337
B
sgRNA+ fraction
puromycin
U87, rep1
U87, rep2
HeLa, rep1
HeLa, rep2
Days post library Infection
C
HeLa
U87
K562
iPSC
MCF7
MDA-MB-231
sgRNAγ, replicate 2
sgRNAγ, replicate 1
lncRNA targeting sgRNAs
non-targeting sgRNAs
D
HeLa
U87
K562
iPSC
MCF7
MDA-MB-231
Screen score, replicate 2
Screen score, replicate 1

Figure S2. CRISPRi growth screens performed in seven cell lines.
A) Schematic of sublibrary divisions of the CRiNCL library. The library was divided into 13 sublibraries based on expression in 7 cell lines to facilitate library cloning and allow for targeted screens. Combinations of sublibraries were selected for screening in each cell line studied as described in Methods. B) Fraction of cells containing the sgRNA library over the course of the U87 and HeLa screens. sgRNA-containing fraction measured as the fraction of high-BFP-expressing cells by flow cytometry. C) sgRNA γ for replicate screens performed in 6 cell lines, as in Figure 1C. Only one replicate was performed for HEK293T. D) Screen scores from replicate screens for individual lncRNA loci. Screen scores were calculated as described in Methods.

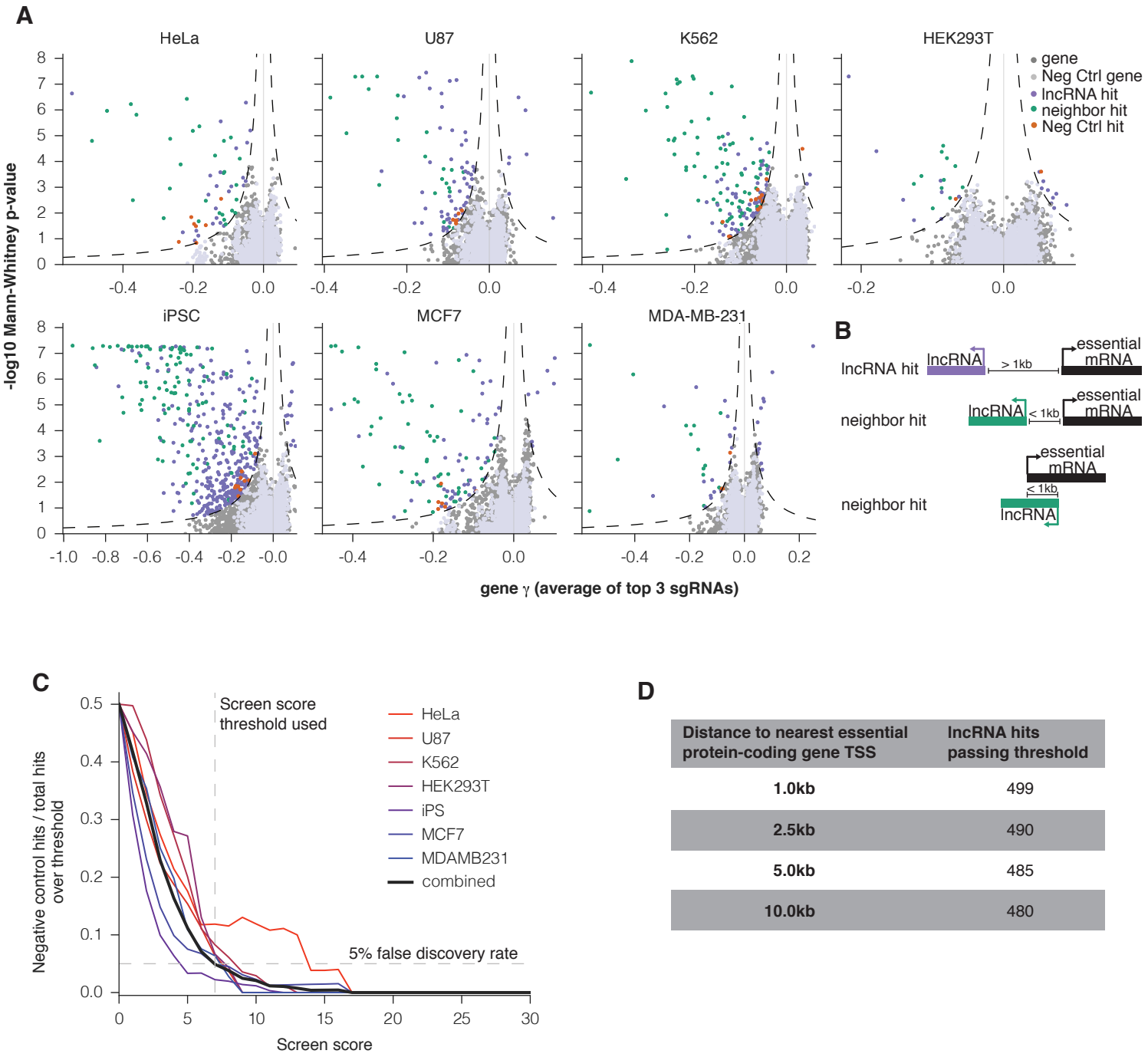

D

Distance to nearest essential protein-coding gene TSS	lncRNA hits passing threshold
1.0kb	499
2.5kb	490
5.0kb	485
10.0kb	480

Figure S3. CRISPRi growth screen results and validation of thresholds used in screen analysis.

A) Volcano plots for screens performed in 7 cell lines, as in Figure 1D. Hits that were considered neighbor hits (see B) are labeled. B) Schematic of definitions of "lncRNA hit" and "neighbor hit." C) Fraction of negative control genes called as hits out of total number of hits above the indicated screen score threshold, calculated for each cell line and the combined dataset. D) Number of lncRNA hits classified after eliminating neighbor hits within the indicated distance from any essential protein-coding gene. A 1.0kb threshold was used for all analysis.

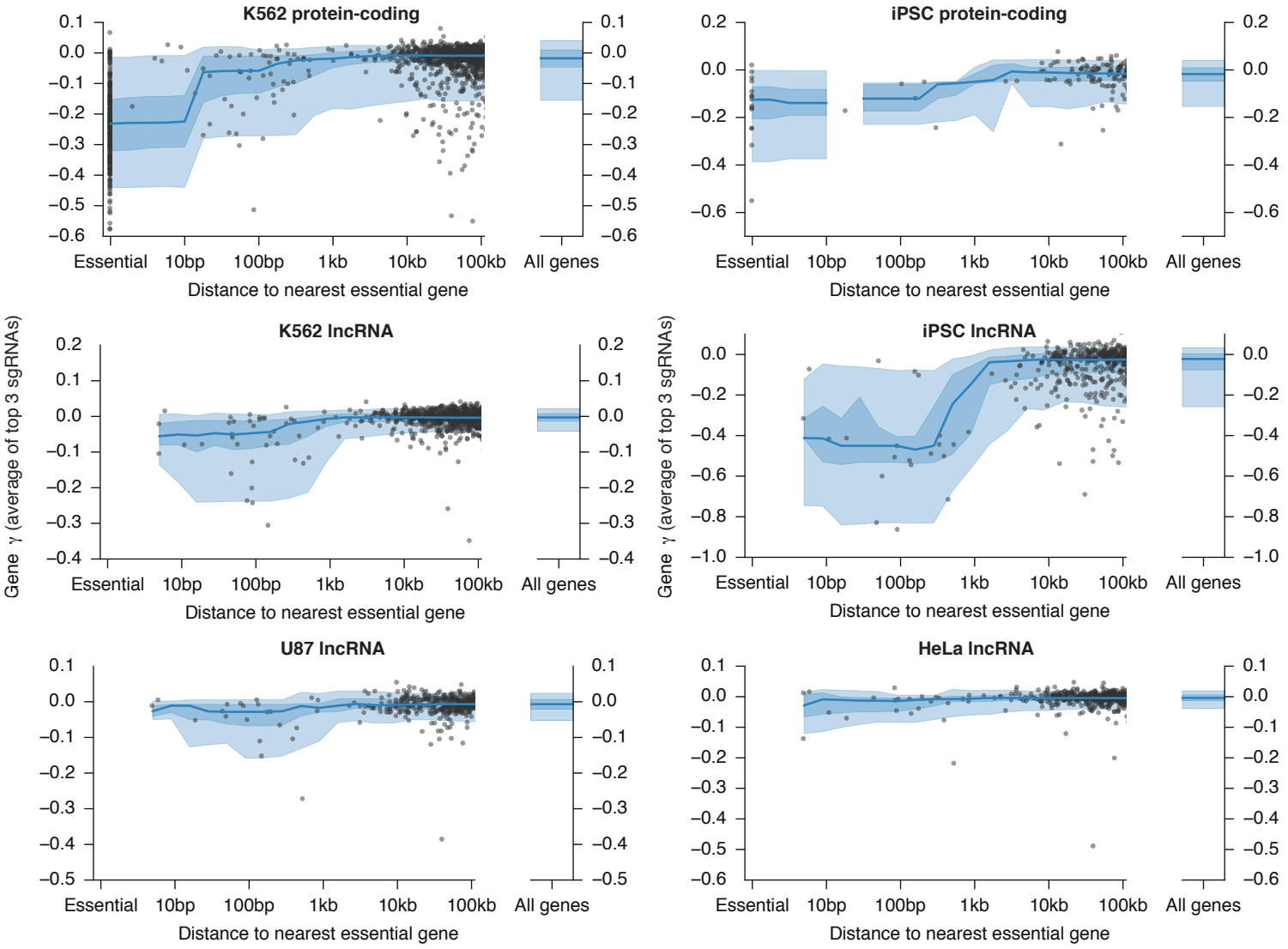

Figure S4. CRISPRi growth phenotypes relative to gold standard essential genes. Distribution of gene γ relative to the nearest gold standard essential protein-coding gene (44). Points indicate individual gene γ scores and blue shaded regions represent 5th, 25th, 50th, 75th, and 95th percentiles of all genes within 10-fold of the position. Screen data plotted are from the indicated protein-coding screens ((35) and Figure S4) or lncRNA screens.

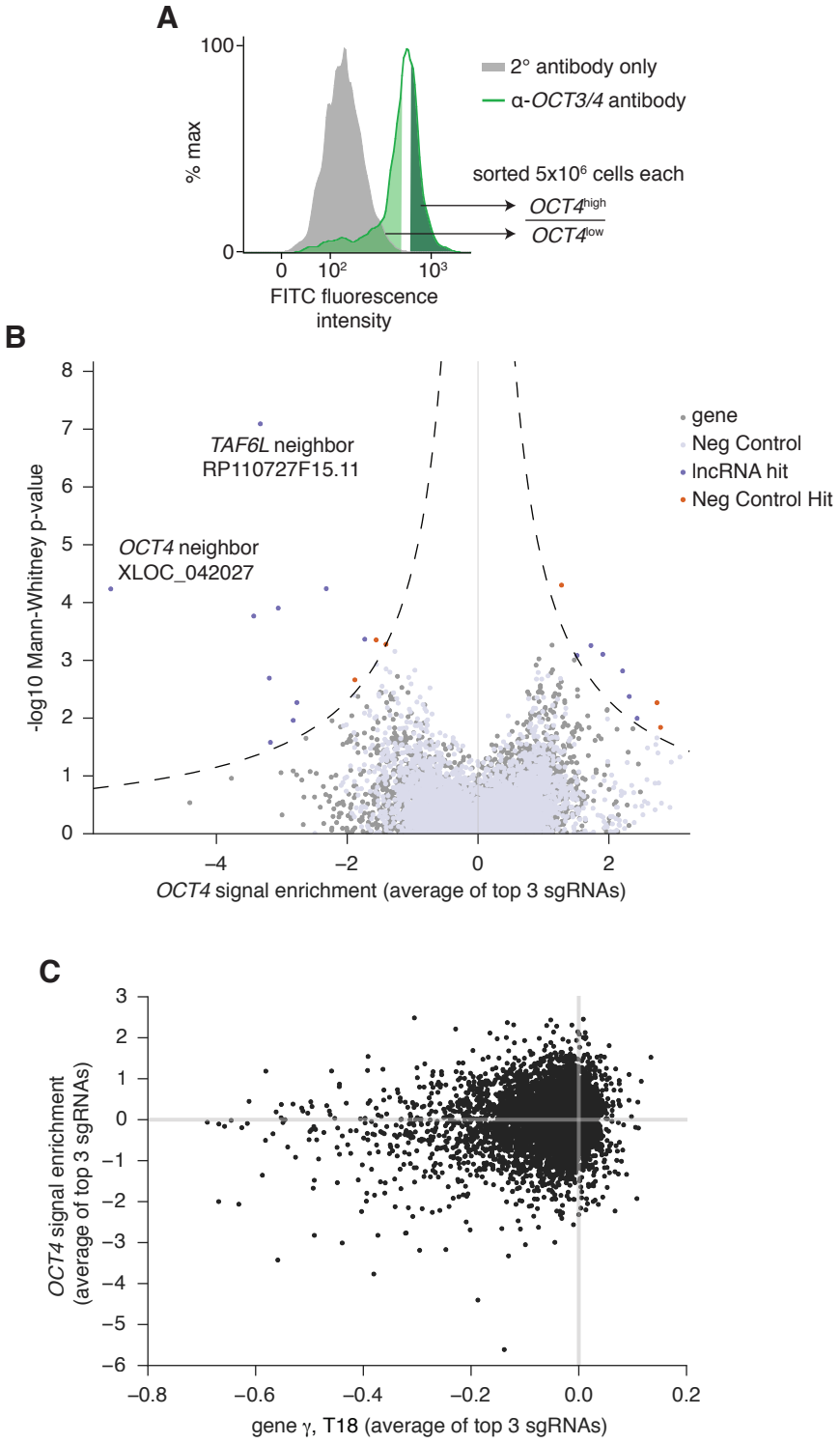

Figure S5. A FACS-based screen for *OCT4* expression identifies genes that modify iPSC differentiation.

A) Representative FACS histogram of *OCT4* staining of iPSCs, with high and low 30% fractions highlighted. $5x10^6$ cells from each fraction were sorted and processed for Illumina sequencing. *OCT4* signal enrichment was calculated as the fraction of each sgRNA present in the high sample versus the low sample. B) Volcano plot of screen results, as in Figure 1D. C) Gene growth phenotypes from iPSC screen compared to *OCT4* signal enrichment. The results suggests that all *OCT4* screen hits also modify cell growth rates, but that most growth screen hits are not accompanied by changes in *OCT4* expression.

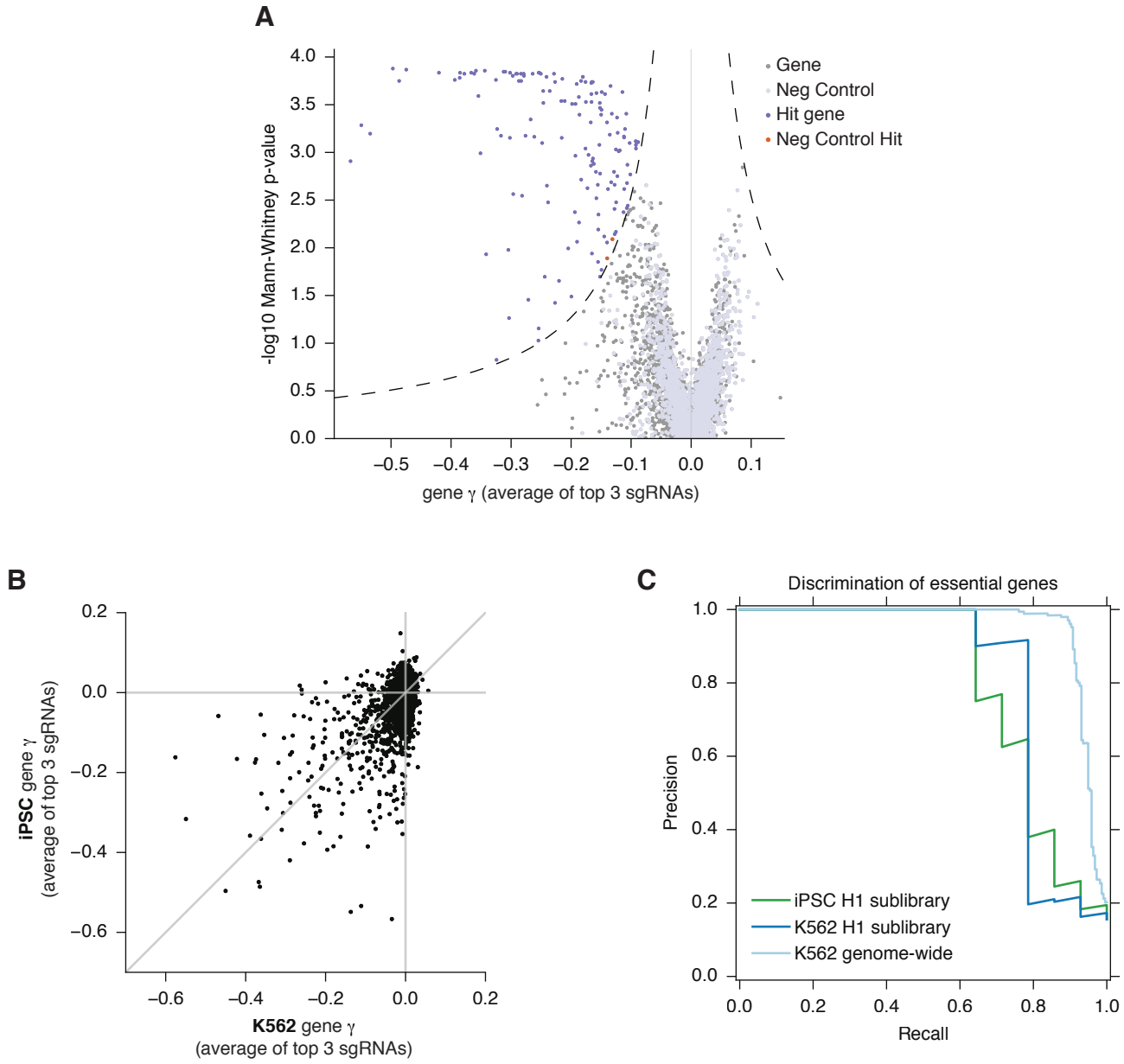

Figure S6. A CRISPRi screen for protein-coding genes that modify growth in iPSC. A) Volcano plot for iPSC screen performed with the hCRISPRi-v2 H1 sublibrary, 5 sgRNAs/gene, displayed as in Figure 1D. Data are the average of two replicate screens. B) Scatter plot of gene γ from growth screens performed in K562 (35) and iPSC. K562 screen was performed with the genome-wide hCRISPRi-v2 library and reanalyzed here using only the H1 5 sgRNAs/gene sublibrary. C) Discrimination of gold-standard essential genes from non-essential genes (44) for K562 and iPSC screens, ranked by gene γ. K562 genome-wide and H1 data were analyzed using the 5 sgRNAs/gene sublibraries.

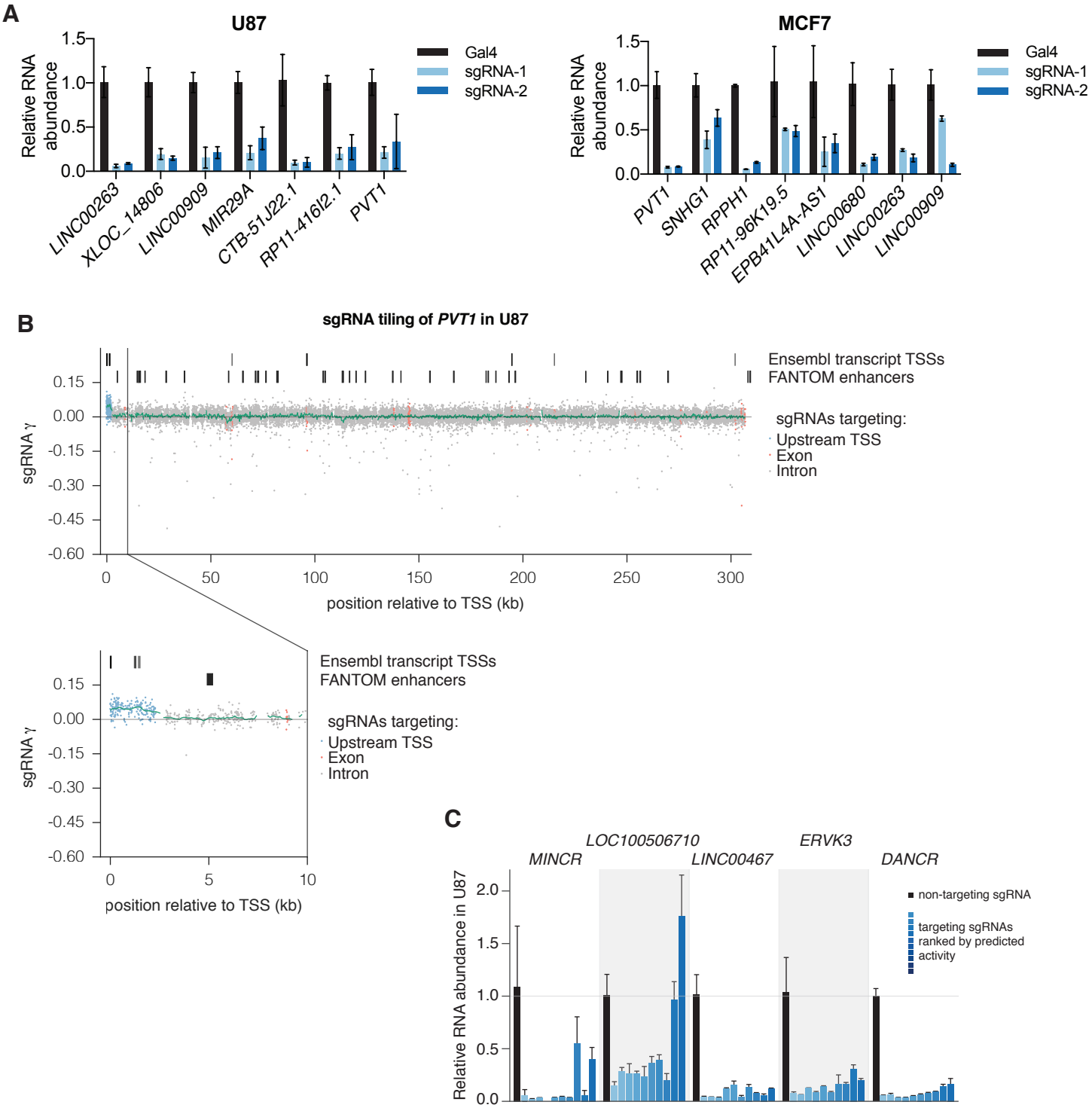

Figure S7. lncRNA CRISPRi produces robust knockdown and is specific to the TSS. A) Relative RNA abundance of lncRNA hits upon knockdown with CRIPSRi. Bars represent mean and standard deviation of 3 biological replicates. B) sgRNA growth phenotypes from tiling screen of *PVT1* in U87 cells by position. sgRNA position was calculated as the genomic coordinate of the protospacer adjacent motif (PAM) relative to the *PVT1* p1 FANTOM TSS. sgRNA γ is the average of two replicates. TSS, exon, and intron are defined as in Figure 2D. Green line represents median phenotype of all sgRNAs within 250bp. C) Relative RNA abundance in U87 of lncRNA genes that were not hits in any cell line, as with Figure F,G.

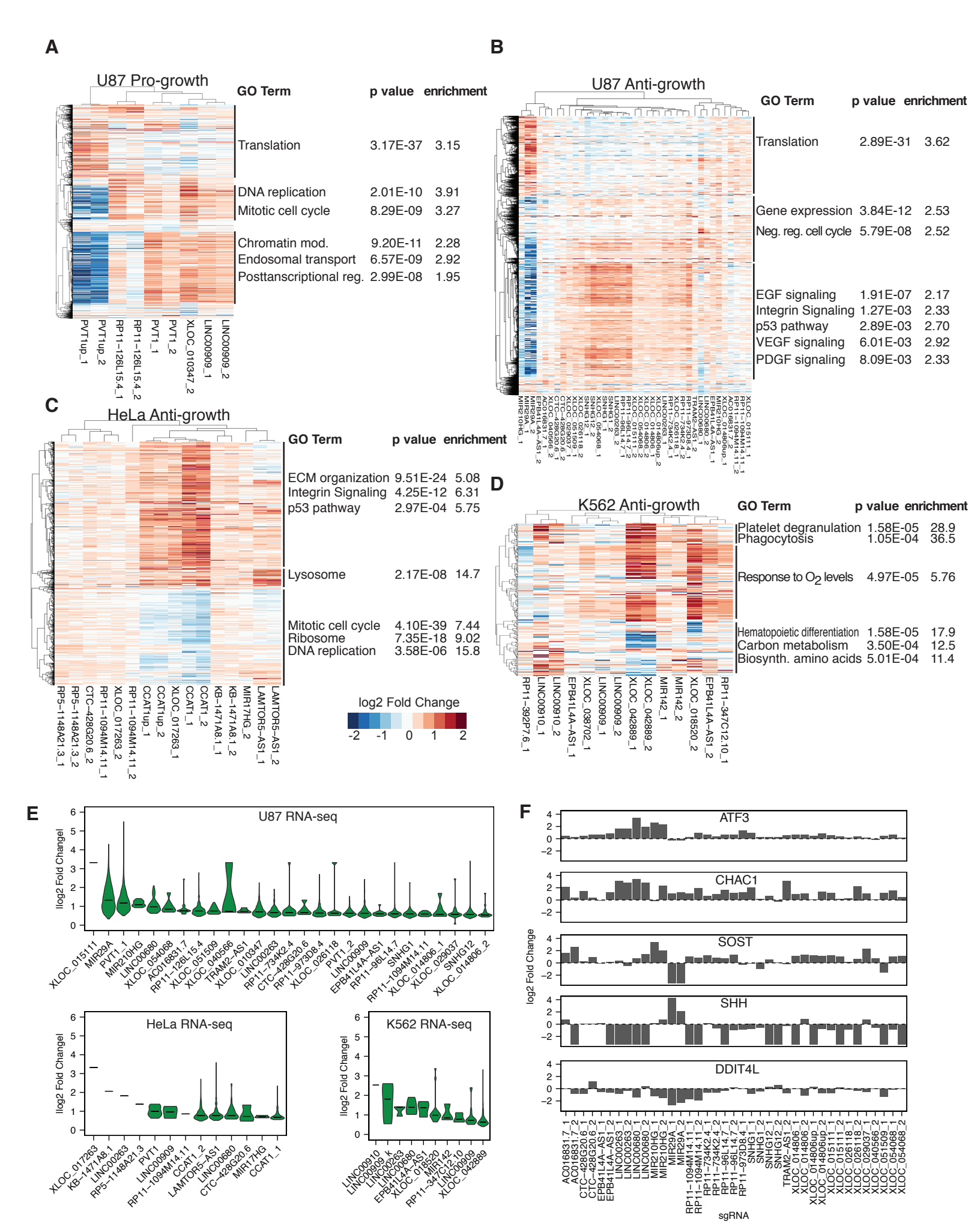
A
U87 Pro-growth
GO Term
p value
enrichment
Translation
3.17E-37
3.15
DNA replication
2.01E-10
3.91
Mitotic cell cycle
8.29E-09
3.27
Chromatin mod.
9.20E-11
2.28
Endosomal transport
6.57E-09
2.92
Posttranscriptional reg.
2.99E-08
1.95
PVT1up_1
PVT1up_2
RP11−126L15.4_1
RP11−126L15.4_2
PVT1_1
PVT1_2
XLOC_010347_2
LINC00909_1
LINC00909_2
B
U87 Anti-growth
GO Term
p value
enrichment
Translation
2.89E-31
3.62
Gene expression
3.84E-12
2.53
Neg. reg. cell cycle
5.79E-08
2.52
EGF signaling
1.91E-07
2.17
Integrin Signaling
1.27E-03
2.33
p53 pathway
2.89E-03
2.70
VEGF signaling
6.01E-03
2.92
PDGF signaling
8.09E-03
2.33
C
HeLa Anti-growth
GO Term
p value
enrichment
ECM organization
9.51E-24
5.08
Integrin Signaling
4.25E-12
6.31
p53 pathway
2.97E-04
5.75
Lysosome
2.17E-08
14.7
Mitotic cell cycle
4.10E-39
7.44
Ribosome
7.35E-18
9.02
DNA replication
3.58E-06
15.8
log2 Fold Change
-2
-1
0
1
2
RP5−1148A21.3_1
RP5−1148A21.3_2
CTC−428G20.6_2
RP11−1094M14.11_1
RP11−1094M14.11_2
XLOC_017263_2
CCAT1up_1
CCAT1up_2
XLOC_017263_1
CCAT1_1
CCAT1_2
KB−1471A8.1_1
KB−1471A8.1_2
MIR17HG_2
LAMTOR5−AS1_1
LAMTOR5−AS1_2
D
K562 Anti-growth
GO Term
p value
enrichment
Platelet degranulation
1.58E-05
28.9
Phagocytosis
1.05E-04
36.5
Response to O_2 levels
4.97E-05
5.76
Hematopoietic differentiation
1.58E-05
17.9
Carbon metabolism
3.50E-04
12.5
Biosynth. amino acids
5.01E-04
11.4
RP11−392P7.6_1
LINC00910_1
LINC00910_2
EPB41L4A−AS1_1
XLOC_038702_1
LINC00909_1
LINC00909_2
XLOC_042889_1
XLOC_042889_2
MIR142_1
MIR142_2
XLOC_018520_2
EPB41L4A−AS1_2
RP11−347C12.10_1
E
U87 RNA-seq
log2 Fold Change
XLOC_015111
MIR29A
PVT1_1
MIR210HG
LINC00680
XLOC_054068
AC016831.7
RP11−126L15.4
XLOC_051509
XLOC_040566
TRAM2−AS1
XLOC_010347
LINC00263
RP11−734K2.4
CTC−428G20.6
RP11−973D8.4
XLOC_026118
PVT1_2
LINC00909
EPB41L4A−AS1
RP11−96L14.7
SNHG1
RP11−1094M14.11
XLOC_014806_1
XLOC_029037
SNHG12
XLOC_014806_2
HeLa RNA-seq
log2 Fold Change
XLOC_017263
KB−1471A8.1
LINC00263
RP5−1148A21.3
PVT1
LINC00909
RP11−1094M14.11
CCAT1_2
LAMTOR5−AS1
LINC00680
CTC−428G20.6
MIR17HG
CCAT1_1
K562 RNA-seq
log2 Fold Change
LINC00910
LINC00909_k
LINC00263
LINC00680
EPB41L4A−AS1
XLOC_018520
MIR142
RP11−347C12.10
LINC00909
XLOC_042889
F
ATF3
CHAC1
SOST
SHH
DDIT4L
log2 Fold Change
AC016831.7_1
AC016831.7_2
CTC−428G20.6_1
CTC−428G20.6_2
EPB41L4A−AS1_1
EPB41L4A−AS1_2
LINC00263_1
LINC00263_2
LINC00680_1
LINC00680_2
MIR210HG_1
MIR210HG_2
MIR29A_1
MIR29A_2
RP11−1094M14.11_1
RP11−1094M14.11_2
RP11−734K2.4_1
RP11−734K2.4_2
RP11−96L14.7_1
RP11−96L14.7_2
RP11−973D8.4_1
SNHG1_1
SNHG1_2
SNHG12_1
SNHG12_2
TRAM2−AS1_2
XLOC_014806_1
XLOC_014806_2
XLOC_014806up_1
XLOC_014806up_2
XLOC_015111_1
XLOC_015111_2
XLOC_026118_1
XLOC_026118_2
XLOC_029037_1
XLOC_040566_2
XLOC_051509_1
XLOC_054068_1
XLOC_054068_2
sgRNA

Figure S8. lncRNA CRISPRi produces co-expressed transcriptome responses. Heatmaps of differentially expressed genes across samples segregated by (A) U87 pro-growth, (B) U87 anti-growth, (C) HeLa anti-growth, (D) K562 anti-growth. Significant gene ontology terms are indicated next to the clusters in which they are enriched, annotated with p value and enrichment. Fold changes are relative to non-targeting controls within the same cell type. E) Distributions of absolute value $\log_2$ fold changes for differentially expressed genes (adj. $p < 0.05$) for each lncRNA knockdown. F) Panel of genes consistently upregulated or downregulated across multiple CRISPRi samples in U87.

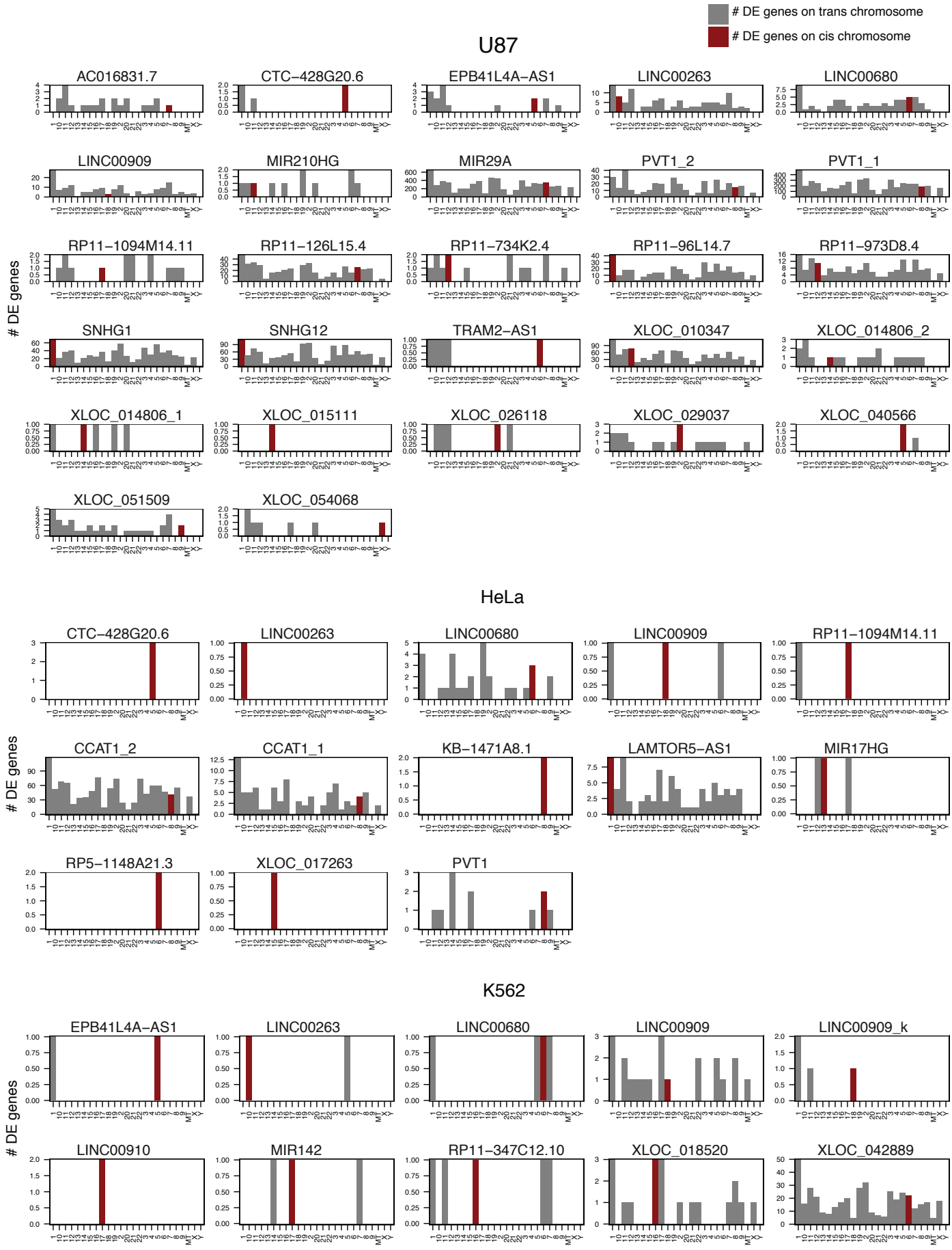
# of Differentially Expressed genes (adj p value < 0.05) at each Chromosome
DE genes on trans chromosome
DE genes on cis chromosome
U87
AC016831.7
CTC−428G20.6
EPB41L4A−AS1
LINC00263
LINC00680
LINC00909
MIR210HG
MIR29A
PVT1_2
PVT1_1
RP11−1094M14.11
RP11−126L15.4
RP11−734K2.4
RP11−96L14.7
RP11−973D8.4
SNHG1
SNHG12
TRAM2−AS1
XLOC_010347
XLOC_014806_2
XLOC_014806_1
XLOC_015111
XLOC_026118
XLOC_029037
XLOC_040566
XLOC_051509
XLOC_054068
DE genes
HeLa
CTC−428G20.6
LINC00263
LINC00680
LINC00909
RP11−1094M14.11
CCAT1_2
CCAT1_1
KB−1471A8.1
LAMTOR5−AS1
MIR17HG
RP5−1148A21.3
XLOC_017263
PVT1
DE genes
K562
EPB41L4A−AS1
LINC00263
LINC00680
LINC00909
LINC00909_k
LINC00910
MIR142
RP11−347C12.10
XLOC_018520
XLOC_042889
DE genes

Figure S9. Chromosome distribution of differentially expressed genes after each lncRNA knockdown. Red bars indicate chromosomes harboring the lncRNAs of interest (*cis*). Gray bars represent chromosomes that do not contain the lncRNAs of interest (*trans*).

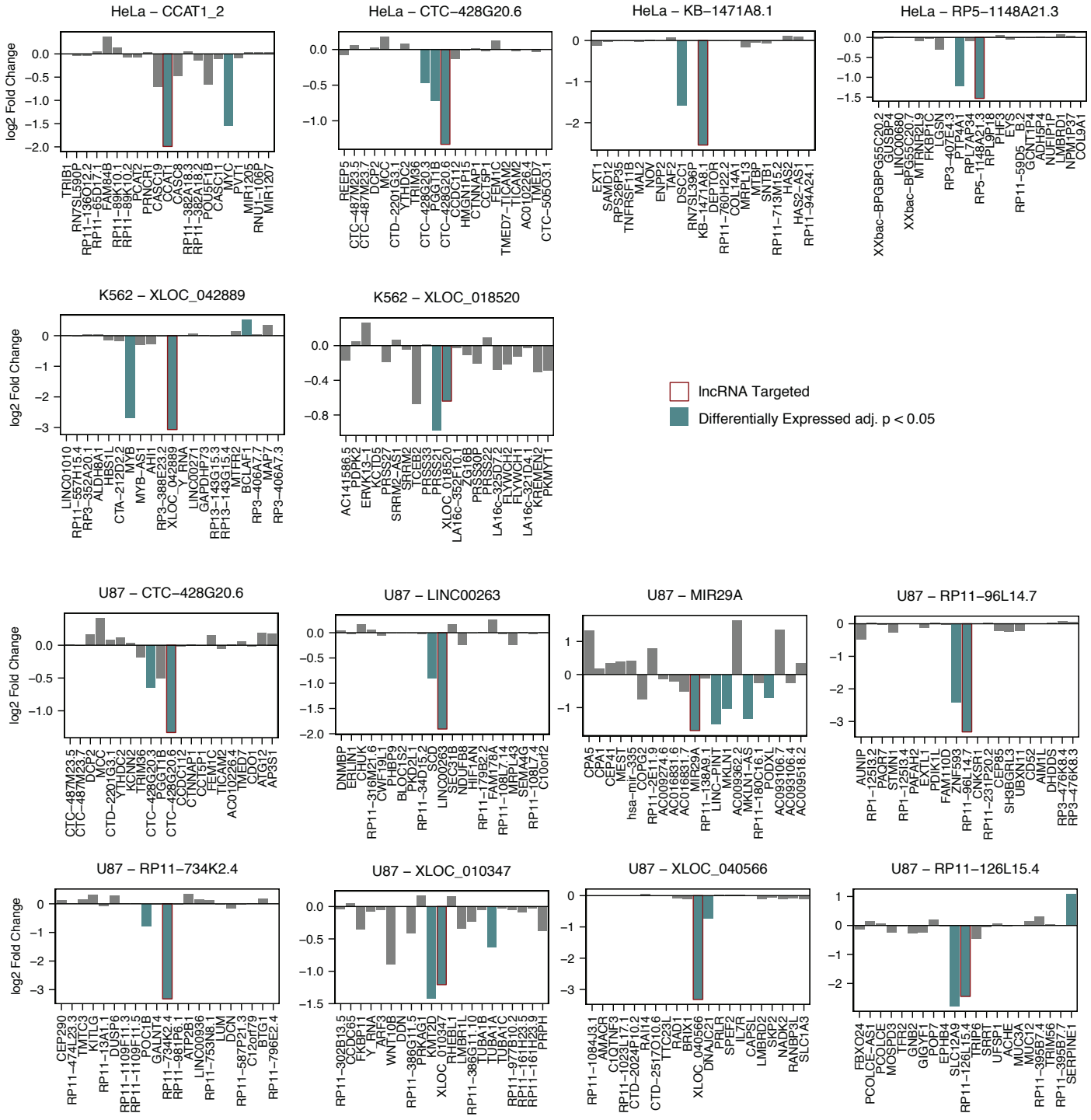

Figure S10. Local transcriptional changes within 20 gene-windows surrounding each lncRNA of interest following CRISPRi knockdown. Red outline indicates targeted lncRNA. Blue bars indicate differentially expressed genes, among the broader set of differentially expressed genes genome-wide (DESeq2 adj. $p < 0.05$) upon knockdown.

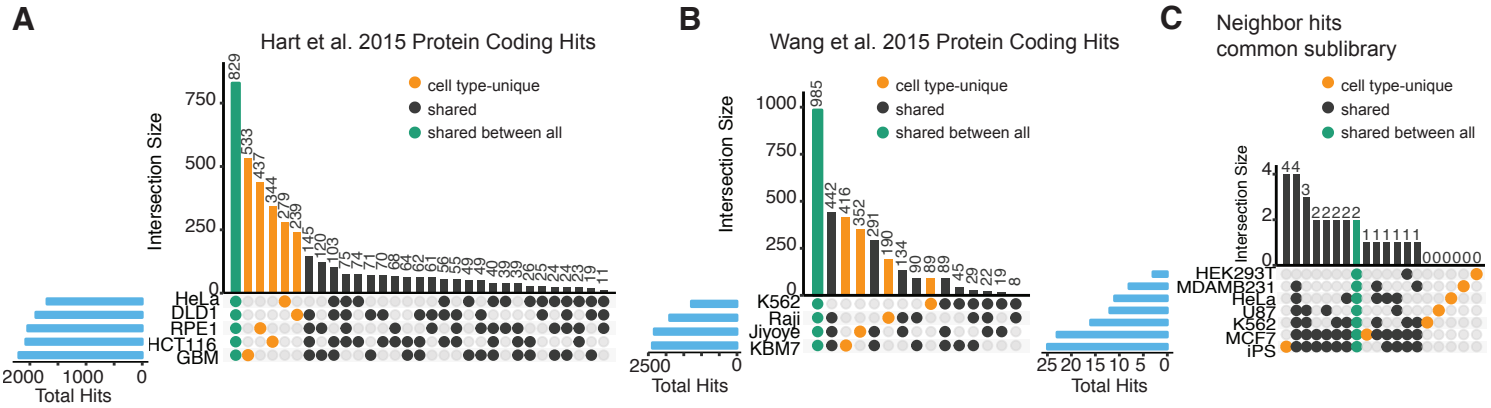
A
Hart et al. 2015 Protein Coding Hits
cell type-unique
shared
shared between all
Intersection Size
HeLa
DLD1
RPE1
HCT116
GBM
Total Hits
B
Wang et al. 2015 Protein Coding Hits
cell type-unique
shared
shared between all
Intersection Size
K562
Raji
Jiyoye
KBM7
Total Hits
C
Neighbor hits
common sublibrary
cell type-unique
shared
shared between all
Intersection Size
HEK293T
MDAMB231
HeLa
U87
K562
MCF7
iPS

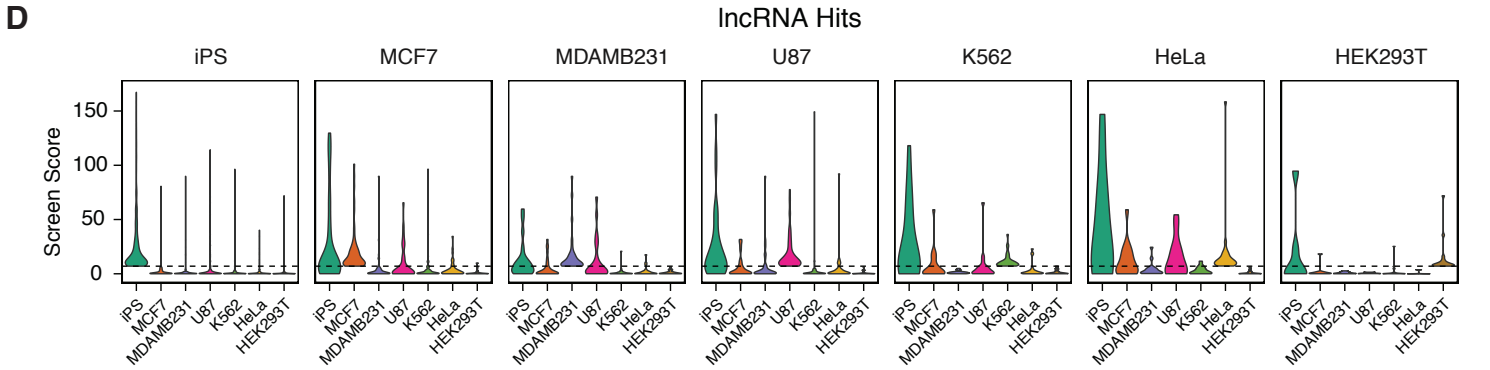
D
lncRNA Hits
iPS
MCF7
MDAMB231
U87
K562
HeLa
HEK293T
Screen Score

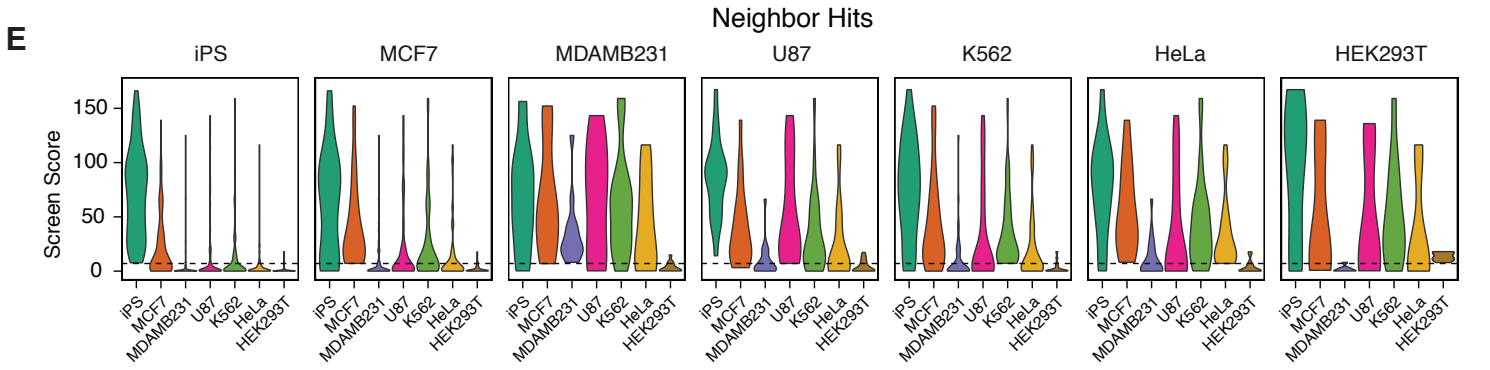
E
Neighbor Hits
iPS
MCF7
MDAMB231
U87
K562
HeLa
HEK293T
Screen Score

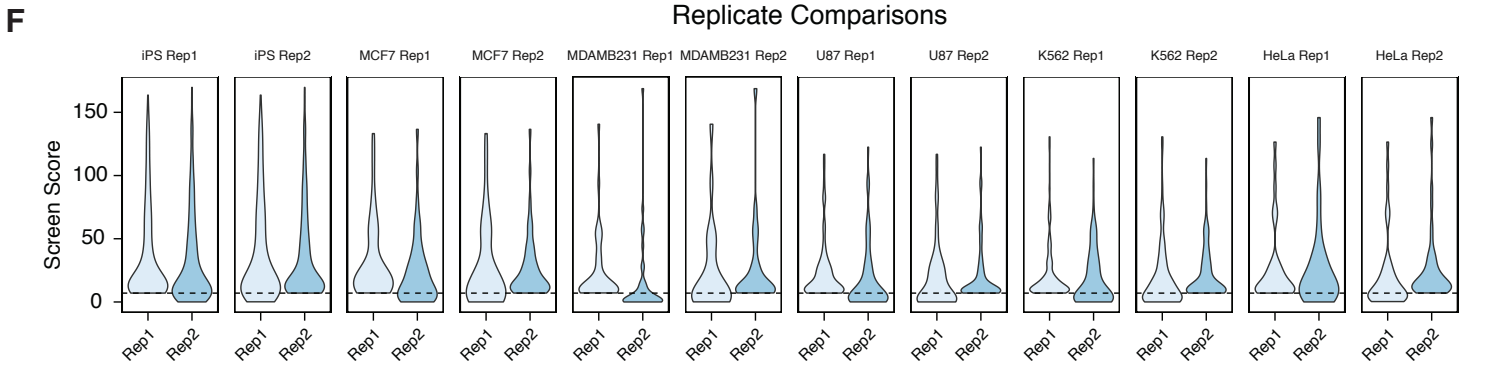
F
Replicate Comparisons
iPS Rep1
iPS Rep2
MCF7 Rep1
MCF7 Rep2
MDAMB231 Rep1
MDAMB231 Rep2
U87 Rep1
U87 Rep2
K562 Rep1
K562 Rep2
HeLa Rep1
HeLa Rep2
Screen Score
Rep1
Rep2

Figure S11. lncRNA hit specificity is greater than essential protein coding gene specificity.
A) Numbers of protein coding gene hits for each set of cell types screened in Hart et al. 2015 and (B) Wang et al. 2015. Wang et al. genes were considered hits if they passed a 5% false discovery threshold set by precision-recall analysis (*44*). C) Numbers of hits in our study that share promoters with essential protein coding genes (neighbor hits). Blue bars indicate total number of hits in each cell type. D) Distributions of screen scores across all cell types, for lncRNAs and (E) "neighbors" that were called hits in each given cell type. F) Distributions of screen scores across both replicates of each cell type, for lncRNAs that would be called as hits in replicate 1 (left) and in replicate 2 (right).

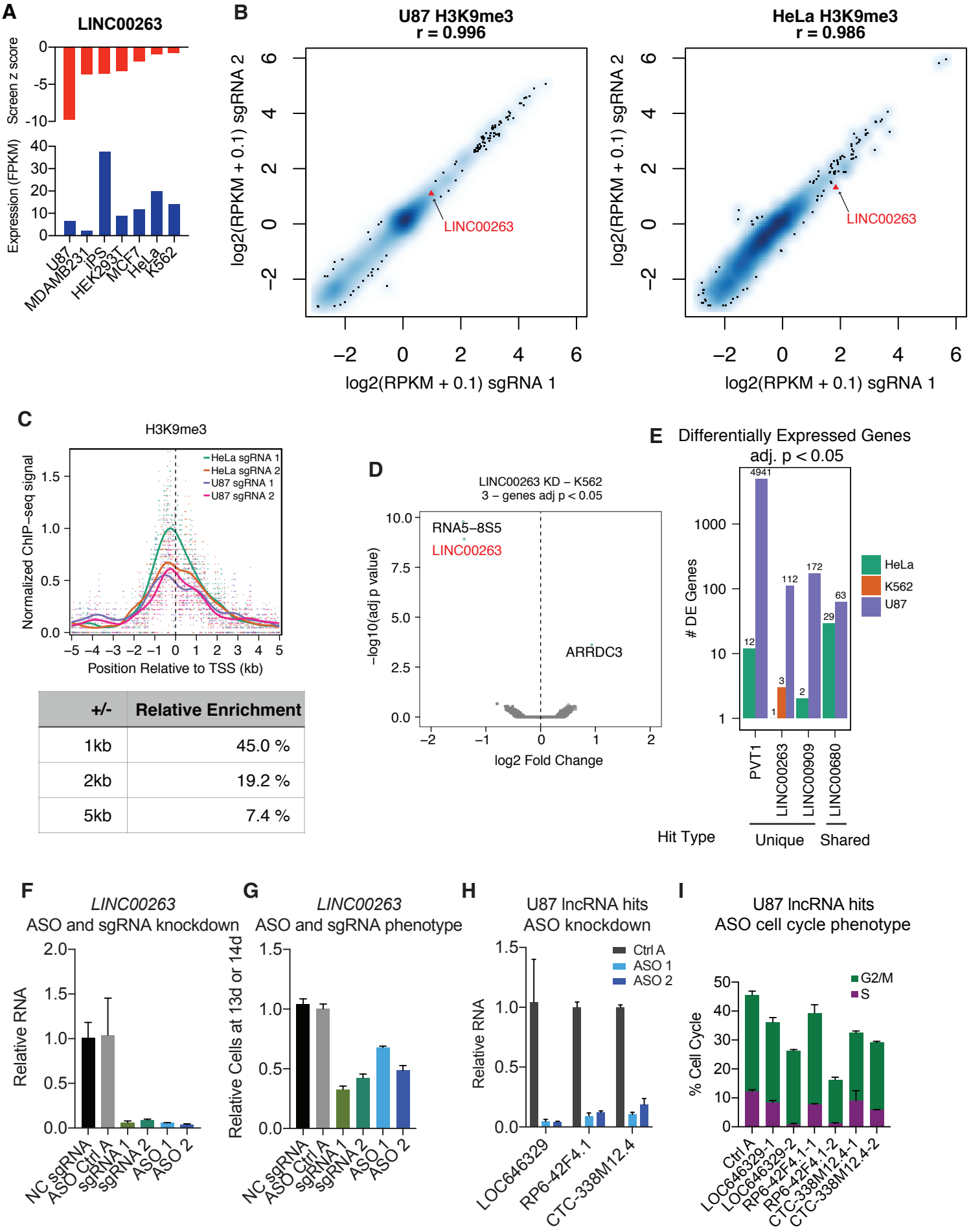

+/-	Relative Enrichment
1kb	45.0 %
2kb	19.2 %
5kb	7.4 %

Figure S12. Cell type-specificity of *LINC00263*.
A) Screen phenotype z scores (red) and expression values (blue) for *LINC00263* across the 7 cell types. B) Reproducibility of H3K9me3 ChIP-seq between sgRNA 1 and sgRNA 2 targeting the TSS of *LINC00263* in U87 (left) and HeLa (right) cells. C) ChIP-seq enrichment of H3K9me3 surrounding the TSS of LINC00263, comparing 2 independent sgRNAs in U87 and HeLa cells. Smoothed lines were obtained by applying a Gaussian kernel smoother against ChIP-seq coverage that had been background subtracted with coverage of H3K9me3 in cells infected with non-targeting control sgRNAs. Signal was then normalized to the peak of the highest smoothed line. Table summarizes relative enrichment of H3K9me3 at various distances beyond the TSS, obtained from the median value of the smoothed lines at each distance. D) Volcano plots for RNA-seq differential expression following infection of *LINC00263* sgRNAs compared to infection of non-targeting sgRNAs in K562 cells. E) Numbers of differentially expressed genes (DESeq2 adj $p < 0.05$) following knockdown of lncRNAs in HeLa, K562, and U87 cells. For each gene, the same sgRNAs were used across the cell types. F) qPCR comparing *LINC00263* knockdown using CRISPRi and ASO. G) Proportion of cells at 14 days post sgRNA infection, or 13 days post ASO transfection against *LINC00263*, relative to control sgRNA or control ASO, respectively. H) qPCR of ASO knockdown of additional lncRNA hits in U87 cells. I) Percentage of cells in S and G2/M phases following ASO knockdown of additional lncRNA hits in U87.

Supplementary Tables:

Table S1 TSS Annotations
Table S2 CRiNCL library sgRNAs
Table S3 Growth screen sgRNA read counts and phenotypes
Table S4 Growth screen gene phenotypes and p-values
Table S5 OCT4 screen sgRNA read counts and phenotypes
Table S6 OCT4 screen gene phenotypes and p-values
Table S7 iPSC protein-coding screen sgRNA and gene phenotypes
Table S8 PVT1 tiling library sgRNAs and phenotypes
Table S9 Differential expression of genes following lncRNA CRISPRi
Table S10 Genomic Properties of lncRNAs
Table S11 Individually cloned sgRNAs and primer pairs used in this study

References

1. S. Djebali, C. A. Davis, A. Merkel, A. Dobin, T. Lassmann, A. Mortazavi, A. Tanzer, J. Lagarde, W. Lin, F. Schlesinger, C. Xue, G. K. Marinov, J. Khatun, B. A. Williams, C. Zaleski, J. Rozowsky, M. Röder, F. Kokocinski, R. F. Abdelhamid, T. Alioto, I. Antoshechkin, M. T. Baer, N. S. Bar, P. Batut, K. Bell, I. Bell, S. Chakrabortty, X. Chen, J. Chrast, J. Curado, T. Derrien, J. Drenkow, E. Dumais, J. Dumais, R. Duttagupta, E. Falconnet, M. Fastuca, K. Fejes-Toth, P. Ferreira, S. Foissac, M. J. Fullwood, H. Gao, D. Gonzalez, A. Gordon, H. Gunawardena, C. Howald, S. Jha, R. Johnson, P. Kapranov, B. King, C. Kingswood, O. J. Luo, E. Park, K. Persaud, J. B. Preall, P. Ribeca, B. Risk, D. Robyr, M. Sammeth, L. Schaffer, L.-H. See, A. Shahab, J. Skancke, A. M. Suzuki, H. Takahashi, H. Tilgner, D. Trout, N. Walters, H. Wang, J. Wrobel, Y. Yu, X. Ruan, Y. Hayashizaki, J. Harrow, M. Gerstein, T. Hubbard, A. Reymond, S. E. Antonarakis, G. Hannon, M. C. Giddings, Y. Ruan, B. Wold, P. Carninci, R. Guigó, T. R. Gingeras, Landscape of transcription in human cells. *Nature* **489**, 101–108 (2012). doi:10.1038/nature11233

2. A. R. R. Forrest, H. Kawaji, M. Rehli, J. Kenneth Baillie, M. J. L. de Hoon, V. Haberle, T. Lassmann, I. V. Kulakovskiy, M. Lizio, M. Itoh, R. Andersson, C. J. Mungall, T. F. Meehan, S. Schmeier, N. Bertin, M. Jørgensen, E. Dimont, E. Arner, C. Schmidl, U. Schaefer, Y. A. Medvedeva, C. Plessy, M. Vitezic, J. Severin, C. A. Semple, Y. Ishizu, R. S. Young, M. Francescatto, I. Alam, D. Albanese, G. M. Altschuler, T. Arakawa, J. A. C. Archer, P. Arner, M. Babina, S. Rennie, P. J. Balwierz, A. G. Beckhouse, S. Pradhan-Bhatt, J. A. Blake, A. Blumenthal, B. Bodega, A. Bonetti, J. Briggs, F. Brombacher, A. Maxwell Burroughs, A. Califano, C. V. Cannistraci, D. Carbajo, Y. Chen, M. Chierici, Y. Ciani, H. C. Clevers, E. Dalla, C. A. Davis, M. Detmar, A. D. Diehl, T. Dohi, F. Drabløs, A. S. B. Edge, M. Edinger, K. Ekwall, M. Endoh, H. Enomoto, M. Fagiolini, L. Fairbairn, H. Fang, M. C. Farach-Carson, G. J. Faulkner, A. V. Favorov, M. E. Fisher, M. C. Frith, R. Fujita, S. Fukuda, C. Furlanello, M. Furuno, J. Furusawa, T. B. Geijtenbeek, A. P. Gibson, T. Gingeras, D. Goldowitz, J. Gough, S. Guhl, R. Guler, S. Gustincich, T. J. Ha, M. Hamaguchi, M. Hara, M. Harbers, J. Harshbarger, A. Hasegawa, Y. Hasegawa, T. Hashimoto, M. Herlyn, K. J. Hitchens, S. J. Ho Sui, O. M. Hofmann, I. Hoof, F. Hori, L. Huminiecki, K. Iida, T. Ikawa, B. R. Jankovic, H. Jia, A. Joshi, G. Jurman, B. Kaczkowski, C. Kai, K. Kaida, A. Kaiho, K. Kajiyama, M. Kanamori-Katayama, A. S. Kasianov, T. Kasukawa, S. Katayama, S. Kato, S. Kawaguchi, H. Kawamoto, Y. I. Kawamura, T. Kawashima, J. S. Kempfle, T. J. Kenna, J. Kere, L. M. Khachigian, T. Kitamura, S. Peter Klinken, A. J. Knox, M. Kojima, S. Kojima, N. Kondo, H. Koseki, S. Koyasu, S. Krampitz, A. Kubosaki, A. T. Kwon, J. F. J. Laros, W. Lee, A. Lennartsson, K. Li, B. Lilje, L. Lipovich, A. Mackay-sim, R. Manabe, J. C. Mar, B. Marchand, A. Mathelier, N. Mejhert, A. Meynert, Y. Mizuno, D. A. de Lima Morais, H. Morikawa, M. Morimoto, K. Moro, E. Motakis, H. Motohashi, C. L. Mummery, M. Murata, S. Nagao-

Sato, Y. Nakachi, F. Nakahara, T. Nakamura, Y. Nakamura, K. Nakazato, E. van Nimwegen, N. Ninomiya, H. Nishiyori, S. Noma, T. Nozaki, S. Ogishima, N. Ohkura, H. Ohmiya, H. Ohno, M. Ohshima, M. Okada-Hatakeyama, Y. Okazaki, V. Orlando, D. A. Ovchinnikov, A. Pain, R. Passier, M. Patrikakis, H. Persson, S. Piazza, J. G. D. Prendergast, O. J. L. Rackham, J. A. Ramilowski, M. Rashid, T. Ravasi, P. Rizzu, M. Roncador, S. Roy, M. B. Rye, E. Saijyo, A. Sajantila, A. Saka, S. Sakaguchi, M. Sakai, H. Sato, H. Satoh, S. Savvi, A. Saxena, C. Schneider, E. A. Schultes, G. G. Schulze-Tanzil, A. Schwegmann, T. Sengstag, G. Sheng, H. Shimoji, Y. Shimoni, J. W. Shin, C. Simon, D. Sugiyama, T. Sugiyama, M. Suzuki, N. Suzuki, R. K. Swoboda, P. A. C. ’t Hoen, M. Tagami, N. Takahashi, J. Takai, H. Tanaka, H. Tatsukawa, Z. Tatum, M. Thompson, H. Toyoda, T. Toyoda, E. Valen, M. van de Wetering, L. M. van den Berg, R. Verardo, D. Vijayan, I. E. Vorontsov, W. W. Wasserman, S. Watanabe, C. A. Wells, L. N. Winteringham, E. Wolvetang, E. J. Wood, Y. Yamaguchi, M. Yamamoto, M. Yoneda, Y. Yonekura, S. Yoshida, S. E. Zabierowski, P. G. Zhang, X. Zhao, S. Zucchelli, K. M. Summers, H. Suzuki, C. O. Daub, J. Kawai, P. Heutink, W. Hide, T. C. Freeman, B. Lenhard, V. B. Bajic, M. S. Taylor, V. J. Makeev, A. Sandelin, D. A. Hume, P. Carninci, Y. Hayashizaki, A promoter-level mammalian expression atlas. *Nature* **507**, 462–470 (2014). doi:10.1038/nature13182

3. I. Ulitsky, D. P. Bartel, lincRNAs: Genomics, evolution, and mechanisms. *Cell* **154**, 26–46 (2013). doi:10.1016/j.cell.2013.06.020

4. J. L. Rinn, H. Y. Chang, Genome regulation by long noncoding RNAs. *Annu. Rev. Biochem.* **81**, 145–166 (2012). doi:10.1146/annurev-biochem-051410-092902

5. C. P. Ponting, P. L. Oliver, W. Reik, Evolution and functions of long noncoding RNAs. *Cell* **136**, 629–641 (2009). doi:10.1016/j.cell.2009.02.006

6. A. R. Bassett, A. Akhtar, D. P. Barlow, A. P. Bird, N. Brockdorff, D. Duboule, A. Ephrussi, A. C. Ferguson-Smith, T. R. Gingeras, W. Haerty, D. R. Higgs, E. A. Miska, C. P. Ponting, Considerations when investigating lncRNA function in vivo. *eLife* **3**, e03058 (2014). doi:10.7554/eLife.03058

7. M. Sauvageau, L. A. Goff, S. Lodato, B. Bonev, A. F. Groff, C. Gerhardinger, D. B. Sanchez-Gomez, E. Hacisuleyman, E. Li, M. Spence, S. C. Liapis, W. Mallard, M. Morse, M. R. Swerdel, M. F. D’Ecclessis, J. C. Moore, V. Lai, G. Gong, G. D. Yancopoulos, D. Frendewey, M. Kellis, R. P. Hart, D. M. Valenzuela, P. Arlotta, J. L. Rinn, Multiple knockout mouse models reveal lincRNAs are required for life and brain development. *eLife* **2**, e01749 (2013). doi:10.7554/eLife.01749

8. V. H. Meller, B. P. Rattner, The roX genes encode redundant male-specific lethal transcripts required for targeting of the MSL complex. *EMBO J.* **21**, 1084–1091 (2002). doi:10.1093/emboj/21.5.1084

9. E. Aparicio-Prat, C. Arnan, I. Sala, N. Bosch, R. Guigó, R. Johnson, DECKO: Single-oligo, dual-CRISPR deletion of genomic elements including long non-coding RNAs. *BMC Genomics* **16**, 846 (2015). doi:10.1186/s12864-015-2086-z

10. T.-T. Ho, N. Zhou, J. Huang, P. Koirala, M. Xu, R. Fung, F. Wu, Y.-Y. Mo, Targeting non-coding RNAs with the CRISPR/Cas9 system in human cell lines. *Nucleic Acids Res.* **43**, 10.1093/nar/gku1198 (2014). doi:10.1093/nar/gku1198

11. T. Wang, J. J. Wei, D. M. Sabatini, E. S. Lander, Genetic screens in human cells using the CRISPR-Cas9 system. *Science* **343**, 80–84 (2014). doi:10.1126/science.1246981

12. O. Shalem, N. E. Sanjana, E. Hartenian, X. Shi, D. A. Scott, T. S. Mikkelsen, D. Heckl, B. L. Ebert, D. E. Root, J. G. Doench, F. Zhang, Genome-scale CRISPR-Cas9 knockout screening in human cells. *Science* **343**, 84–87 (2014). doi:10.1126/science.1247005

13. J. Shi, E. Wang, J. P. Milazzo, Z. Wang, J. B. Kinney, C. R. Vakoc, Discovery of cancer drug targets by CRISPR-Cas9 screening of protein domains. *Nat. Biotechnol.* **33**, 661–667 (2015). doi:10.1038/nbt.3235

14. Y. Yin, P. Yan, J. Lu, G. Song, Y. Zhu, Z. Li, Y. Zhao, B. Shen, X. Huang, H. Zhu, S. H. Orkin, X. Shen, Opposing roles for the lncRNA haunt and its genomic locus in regulating HOXA gene activation during embryonic stem cell differentiation. *Cell Stem Cell* **16**, 504–516 (2015). doi:10.1016/j.stem.2015.03.007

15. V. R. Paralkar, C. C. Taborda, P. Huang, Y. Yao, A. V. Kossenkov, R. Prasad, J. Luan, J. O. J. Davies, J. R. Hughes, R. C. Hardison, G. A. Blobel, M. J. Weiss, Unlinking an lncRNA from its associated cis element. *Mol. Cell* **62**, 104–110 (2016). doi:10.1016/j.molcel.2016.02.029

16. A. F. Groff, D. B. Sanchez-Gomez, M. M. L. Soruco, C. Gerhardinger, A. R. Barutcu, E. Li, L. Elcavage, O. Plana, L. V. Sanchez, J. C. Lee, M. Sauvageau, J. L. Rinn, In vivo characterization of Linc-p21 reveals functional cis-regulatory DNA elements. *Cell Rep.* **16**, 2178–2186 (2016). doi:10.1016/j.celrep.2016.07.050

17. S. Zhu, W. Li, J. Liu, C.-H. Chen, Q. Liao, P. Xu, H. Xu, T. Xiao, Z. Cao, J. Peng, P. Yuan, M. Brown, X. S. Liu, W. Wei, Genome-scale deletion screening of human long non-coding RNAs using a paired-guide RNA CRISPR-Cas9 library. *Nat. Biotechnol.* 10.1038/nbt.3715 (2016). doi:10.1038/nbt.3715

18. M. Guttman, J. Donaghey, B. W. Carey, M. Garber, J. K. Grenier, G. Munson, G. Young, A. B. Lucas, R. Ach, L. Bruhn, X. Yang, I. Amit, A. Meissner, A. Regev, J. L. Rinn, D. E. Root, E. S. Lander, lincRNAs act in the circuitry controlling pluripotency and differentiation. *Nature* **477**, 295–300 (2011). doi:10.1038/nature10398

19. N. Lin, K.-Y. Chang, Z. Li, K. Gates, Z. A. Rana, J. Dang, D. Zhang, T. Han, C.-S. Yang, T. J. Cunningham, S. R. Head, G. Duester, P. D. S. Dong, T. M. Rana, An evolutionarily

conserved long noncoding RNA TUNA controls pluripotency and neural lineage commitment. *Mol. Cell* **53**, 1005–1019 (2014). doi:10.1016/j.molcel.2014.01.021

20. B. Adamson, A. Smogorzewska, F. D. Sigoillot, R. W. King, S. J. Elledge, A genome-wide homologous recombination screen identifies the RNA-binding protein RBMX as a component of the DNA-damage response. *Nat. Cell Biol.* **14**, 318–328 (2012). doi:10.1038/ncb2426

21. Y. Zeng, B. R. Cullen, RNA interference in human cells is restricted to the cytoplasm. *RNA* **8**, 855–860 (2002). doi:10.1017/S1355838202020071

22. L. A. Gilbert, M. H. Larson, L. Morsut, Z. Liu, G. A. Brar, S. E. Torres, N. Stern-Ginossar, O. Brandman, E. H. Whitehead, J. A. Doudna, W. A. Lim, J. S. Weissman, L. S. Qi, CRISPR-mediated modular RNA-guided regulation of transcription in eukaryotes. *Cell* **154**, 442–451 (2013). doi:10.1016/j.cell.2013.06.044

23. L. A. Gilbert, M. A. Horlbeck, B. Adamson, J. E. Villalta, Y. Chen, E. H. Whitehead, C. Guimaraes, B. Panning, H. L. Ploegh, M. C. Bassik, L. S. Qi, M. Kampmann, J. S. Weissman, Genome-scale CRISPR-mediated control of gene repression and activation. *Cell* **159**, 647–661 (2014). doi:10.1016/j.cell.2014.09.029

24. L. S. Qi, M. H. Larson, L. A. Gilbert, J. A. Doudna, J. S. Weissman, A. P. Arkin, W. A. Lim, Repurposing CRISPR as an RNA-guided platform for sequence-specific control of gene expression. *Cell* **152**, 1173–1183 (2013). doi:10.1016/j.cell.2013.02.022

25. H. Nishimasu, L. Cong, W. X. Yan, F. A. Ran, B. Zetsche, Y. Li, A. Kurabayashi, R. Ishitani, F. Zhang, O. Nureki, Crystal structure of *Staphylococcus aureus* Cas9. *Cell* **162**, 1113–1126 (2015). doi:10.1016/j.cell.2015.08.007

26. J. M. Engreitz, J. E. Haines, G. Munson, J. Chen, E. M. Perez, http://biorxiv.org/content/early/2016/04/28/050948 (2016).

27. A. E. Kornienko, P. M. Guenzl, D. P. Barlow, F. M. Pauler, Gene regulation by the act of long non-coding RNA transcription. *BMC Biol.* **11**, 59 (2013). doi:10.1186/1741-7007-11-59

28. U. A. Ørom, T. Derrien, M. Beringer, K. Gumireddy, A. Gardini, G. Bussotti, F. Lai, M. Zytnicki, C. Notredame, Q. Huang, R. Guigo, R. Shiekhattar, Long noncoding RNAs with enhancer-like function in human cells. *Cell* **143**, 46–58 (2010). doi:10.1016/j.cell.2010.09.001

29. W. Li, D. Notani, Q. Ma, B. Tanasa, E. Nunez, A. Y. Chen, D. Merkurjev, J. Zhang, K. Ohgi, X. Song, S. Oh, H.-S. Kim, C. K. Glass, M. G. Rosenfeld, Functional roles of enhancer RNAs for oestrogen-dependent transcriptional activation. *Nature* **498**, 516–520 (2013). doi:10.1038/nature12210

30. C. P. Fulco, M. Munschauer, R. Anyoha, G. Munson, S. R. Grossman, E. M. Perez, M. Kane, B. Cleary, E. S. Lander, J. M. Engreitz, Systematic mapping of functional enhancer-promoter connections with CRISPR interference. *Science* **354**, 769–773 (2016). doi:10.1126/science.aag2445

31. P. I. Thakore, A. M. D'Ippolito, L. Song, A. Safi, N. K. Shivakumar, A. M. Kabadi, T. E. Reddy, G. E. Crawford, C. A. Gersbach, Highly specific epigenome editing by CRISPR-Cas9 repressors for silencing of distal regulatory elements. *Nat. Methods* **12**, 1143–1149 (2015). doi:10.1038/nmeth.3630

32. A. Amabile, A. Migliara, P. Capasso, M. Biffi, D. Cittaro, L. Naldini, A. Lombardo, Inheritable silencing of endogenous genes by hit-and-run targeted epigenetic editing. *Cell* **167**, 219–232.e14 (2016). doi:10.1016/j.cell.2016.09.006

33. M. A. Mandegar, N. Huebsch, E. B. Frolov, E. Shin, A. Truong, M. P. Olvera, A. H. Chan, Y. Miyaoka, K. Holmes, C. I. Spencer, L. M. Judge, D. E. Gordon, T. V. Eskildsen, J. E. Villalta, M. A. Horlbeck, L. A. Gilbert, N. J. Krogan, S. P. Sheikh, J. S. Weissman, L. S. Qi, P.-L. So, B. R. Conklin, CRISPR interference efficiently induces specific and reversible gene silencing in human iPSCs. *Cell Stem Cell* **18**, 541–553 (2016). doi:10.1016/j.stem.2016.01.022

34. C. J. Braun, P. M. Bruno, M. A. Horlbeck, L. A. Gilbert, J. S. Weissman, M. T. Hemann, Versatile in vivo regulation of tumor phenotypes by dCas9-mediated transcriptional perturbation. *Proc. Natl. Acad. Sci. U.S.A.* **113**, E3892–E3900 (2016). doi:10.1073/pnas.1600582113

35. M. A. Horlbeck, L. A. Gilbert, J. E. Villalta, B. Adamson, R. A. Pak, Y. Chen, A. P. Fields, C. Y. Park, J. E. Corn, M. Kampmann, J. S. Weissman, Compact and highly active next-generation libraries for CRISPR-mediated gene repression and activation. *eLife* **5**, e19760 (2016). doi:10.7554/eLife.19760

36. K. Takahashi, K. Tanabe, M. Ohnuki, M. Narita, T. Ichisaka, K. Tomoda, S. Yamanaka, Induction of pluripotent stem cells from adult human fibroblasts by defined factors. *Cell* **131**, 861–872 (2007). doi:10.1016/j.cell.2007.11.019

37. M. N. Cabili, C. Trapnell, L. Goff, M. Koziol, B. Tazon-Vega, A. Regev, J. L. Rinn, Integrative annotation of human large intergenic noncoding RNAs reveals global properties and specific subclasses. *Genes Dev.* **25**, 1915–1927 (2011). doi:10.1101/gad.17446611

38. M. K. Iyer, Y. S. Niknafs, R. Malik, U. Singhal, A. Sahu, Y. Hosono, T. R. Barrette, J. R. Prensner, J. R. Evans, S. Zhao, A. Poliakov, X. Cao, S. M. Dhanasekaran, Y.-M. Wu, D. R. Robinson, D. G. Beer, F. Y. Feng, H. K. Iyer, A. M. Chinnaiyan, The landscape of long noncoding RNAs in the human transcriptome. *Nat. Genet.* **47**, 199–208 (2015). doi:10.1038/ng.3192

39. A. Yates, W. Akanni, M. R. Amode, D. Barrell, K. Billis, D. Carvalho-Silva, C. Cummins, P. Clapham, S. Fitzgerald, L. Gil, C. G. Girón, L. Gordon, T. Hourlier, S. E. Hunt, S. H. Janacek, N. Johnson, T. Juettemann, S. Keenan, I. Lavidas, F. J. Martin, T. Maurel, W. McLaren, D. N. Murphy, R. Nag, M. Nuhn, A. Parker, M. Patricio, M. Pignatelli, M. Rahtz, H. S. Riat, D. Sheppard, K. Taylor, A. Thormann, A. Vullo, S. P. Wilder, A. Zadissa, E. Birney, J. Harrow, M. Muffato, E. Perry, M. Ruffier, G. Spudich, S. J. Trevanion, F. Cunningham, B. L. Aken, D. R. Zerbino, P. Flicek, Ensembl 2016. *Nucleic Acids Res.* **44**, D710–D716 (2015). doi:10.1093/nar/gkv1157

40. ENCODE Project Consortium, The ENCODE (ENCyclopedia Of DNA Elements) Project. *Science* **306**, 636–640 (2004). doi:10.1126/science.1105136

41. F. R. Kreitzer *et al.*, A robust method to derive functional neural crest cells from human pluripotent stem cells. *Am. J. Stem Cells* **2**, 119–131 (2013).

42. S. J. Liu, T. J. Nowakowski, A. A. Pollen, J. H. Lui, M. A. Horlbeck, F. J. Attenello, D. He, J. S. Weissman, A. R. Kriegstein, A. A. Diaz, D. A. Lim, Single-cell analysis of long non-coding RNAs in the developing human neocortex. *Genome Biol.* **17**, 67 (2016). doi:10.1186/s13059-016-0932-1

43. M. Kampmann, M. C. Bassik, J. S. Weissman, Integrated platform for genome-wide screening and construction of high-density genetic interaction maps in mammalian cells. *Proc. Natl. Acad. Sci. U.S.A.* **110**, E2317–E2326 (2013). doi:10.1073/pnas.1307002110

44. T. Hart, K. R. Brown, F. Sircoulomb, R. Rottapel, J. Moffat, Measuring error rates in genomic perturbation screens: Gold standards for human functional genomics. *Mol. Syst. Biol.* **10**, 733 (2014). doi:10.15252/msb.20145216

45. Y.-Y. Tseng *et al.*, PVT1 dependence in cancer with MYC copy-number increase. *Nature* **512**, 82–86 (2014).

46. T. Wang, K. Birsoy, N. W. Hughes, K. M. Krupczak, Y. Post, J. J. Wei, E. S. Lander, D. M. Sabatini, Identification and characterization of essential genes in the human genome. *Science* **350**, 1096–1101 (2015). doi:10.1126/science.aac7041

47. T. Hart, M. Chandrashekhar, M. Aregger, Z. Steinhart, K. R. Brown, G. MacLeod, M. Mis, M. Zimmermann, A. Fradet-Turcotte, S. Sun, P. Mero, P. Dirks, S. Sidhu, F. P. Roth, O. S. Rissland, D. Durocher, S. Angers, J. Moffat, High-resolution CRISPR screens reveal fitness genes and genotype-specific cancer liabilities. *Cell* **163**, 1515–1526 (2015). doi:10.1016/j.cell.2015.11.015

48. R. Andersson, C. Gebhard, I. Miguel-Escalada, I. Hoof, J. Bornholdt, M. Boyd, Y. Chen, X. Zhao, C. Schmidl, T. Suzuki, E. Ntini, E. Arner, E. Valen, K. Li, L. Schwarzfischer, D. Glatz, J. Raithel, B. Lilje, N. Rapin, F. O. Bagger, M. Jørgensen, P. R. Andersen, N. Bertin, O. Rackham, A. M. Burroughs, J. K. Baillie, Y. Ishizu, Y. Shimizu, E. Furuhata, S. Maeda, Y. Negishi, C. J. Mungall, T. F. Meehan, T. Lassmann, M. Itoh, H. Kawaji, N.

Kondo, J. Kawai, A. Lennartsson, C. O. Daub, P. Heutink, D. A. Hume, T. H. Jensen, H. Suzuki, Y. Hayashizaki, F. Müller, T. F. A. N. T. O. M. Consortium, A. R. R. Forrest, P. Carninci, M. Rehli, A. Sandelin, An atlas of active enhancers across human cell types and tissues. *Nature* **507**, 455–461 (2014). doi:10.1038/nature12787

49. A. Visel, S. Minovitsky, I. Dubchak, L. A. Pennacchio, VISTA Enhancer Browser–a database of tissue-specific human enhancers. *Nucleic Acids Res.* **35**, D88–D92 (2007). doi:10.1093/nar/gkl822

50. X. Yan, Z. Hu, Y. Feng, X. Hu, J. Yuan, S. D. Zhao, Y. Zhang, L. Yang, W. Shan, Q. He, L. Fan, L. E. Kandalaft, J. L. Tanyi, C. Li, C.-X. Yuan, D. Zhang, H. Yuan, K. Hua, Y. Lu, D. Katsaros, Q. Huang, K. Montone, Y. Fan, G. Coukos, J. Boyd, A. K. Sood, T. Rebbeck, G. B. Mills, C. V. Dang, L. Zhang, Comprehensive genomic characterization of long non-coding RNAs across human cancers. *Cancer Cell* **28**, 529–540 (2015). doi:10.1016/j.ccell.2015.09.006

51. D. Hnisz, B. J. Abraham, T. I. Lee, A. Lau, V. Saint-André, A. A. Sigova, H. A. Hoke, R. A. Young, Super-enhancers in the control of cell identity and disease. *Cell* **155**, 934–947 (2013). doi:10.1016/j.cell.2013.09.053

52. J. Chen, A. A. Shishkin, X. Zhu, S. Kadri, I. Maza, M. Guttman, J. H. Hanna, A. Regev, M. Garber, Evolutionary analysis across mammals reveals distinct classes of long non-coding RNAs. *Genome Biol.* **17**, 19 (2016). doi:10.1186/s13059-016-0880-9

53. K. C. Wang, Y. W. Yang, B. Liu, A. Sanyal, R. Corces-Zimmerman, Y. Chen, B. R. Lajoie, A. Protacio, R. A. Flynn, R. A. Gupta, J. Wysocka, M. Lei, J. Dekker, J. A. Helms, H. Y. Chang, A long noncoding RNA maintains active chromatin to coordinate homeotic gene expression. *Nature* **472**, 120–124 (2011). doi:10.1038/nature09819

54. W. Ma, F. Ay, C. Lee, G. Gulsoy, X. Deng, S. Cook, J. Hesson, C. Cavanaugh, C. B. Ware, A. Krumm, J. Shendure, C. A. Blau, C. M. Disteche, W. S. Noble, Z. Duan, Fine-scale chromatin interaction maps reveal the cis-regulatory landscape of human lincRNA genes. *Nat. Methods* **12**, 71–78 (2015). doi:10.1038/nmeth.3205

55. J. M. Engreitz, A. Pandya-Jones, P. McDonel, A. Shishkin, K. Sirokman, C. Surka, S. Kadri, J. Xing, A. Goren, E. S. Lander, K. Plath, M. Guttman, The Xist lncRNA exploits three-dimensional genome architecture to spread across the X chromosome. *Science* **341**, 1237973 (2013). doi:10.1126/science.1237973

56. A. Necsulea, M. Soumillon, M. Warnefors, A. Liechti, T. Daish, U. Zeller, J. C. Baker, F. Grützner, H. Kaessmann, The evolution of lncRNA repertoires and expression patterns in tetrapods. *Nature* **505**, 635–640 (2014). doi:10.1038/nature12943

57. A. D. Ramos, R. E. Andersen, S. J. Liu, T. J. Nowakowski, S. J. Hong, C. C. Gertz, R. D. Salinas, H. Zarabi, A. R. Kriegstein, D. A. Lim, The long noncoding RNA Pnky regulates

neuronal differentiation of embryonic and postnatal neural stem cells. *Cell Stem Cell* **16**, 439–447 (2015). doi:10.1016/j.stem.2015.02.007

58. M. Kretz, Z. Siprashvili, C. Chu, D. E. Webster, A. Zehnder, K. Qu, C. S. Lee, R. J. Flockhart, A. F. Groff, J. Chow, D. Johnston, G. E. Kim, R. C. Spitale, R. A. Flynn, G. X. Y. Zheng, S. Aiyer, A. Raj, J. L. Rinn, H. Y. Chang, P. A. Khavari, Control of somatic tissue differentiation by the long non-coding RNA TINCR. *Nature* **493**, 231–235 (2013). doi:10.1038/nature11661

59. T. Gutschner, M. Hammerle, M. Eissmann, J. Hsu, Y. Kim, G. Hung, A. Revenko, G. Arun, M. Stentrup, M. Gross, M. Zornig, A. R. MacLeod, D. L. Spector, S. Diederichs, The noncoding RNA MALAT1 is a critical regulator of the metastasis phenotype of lung cancer cells. *Cancer Res.* **73**, 1180–1189 (2013). doi:10.1158/0008-5472.CAN-12-2850

60. R. A. Gupta, N. Shah, K. C. Wang, J. Kim, H. M. Horlings, D. J. Wong, M.-C. Tsai, T. Hung, P. Argani, J. L. Rinn, Y. Wang, P. Brzoska, B. Kong, R. Li, R. B. West, M. J. van de Vijver, S. Sukumar, H. Y. Chang, Long non-coding RNA HOTAIR reprograms chromatinstate to promote cancer metastasis. *Nature* **464**, 1071–1076 (2011). doi:10.1038/nature08975

61. J. A. Briggs, E. J. Wolvetang, J. S. Mattick, J. L. Rinn, G. Barry, Mechanisms of long non-coding RNAs in mammalian nervous system development, plasticity, disease, and evolution. *Neuron* **88**, 861–877 (2015). doi:10.1016/j.neuron.2015.09.045

62. C. Trapnell, B. A. Williams, G. Pertea, A. Mortazavi, G. Kwan, M. J. van Baren, S. L. Salzberg, B. J. Wold, L. Pachter, Transcript assembly and quantification by RNA-Seq reveals unannotated transcripts and isoform switching during cell differentiation. *Nat. Biotechnol.* **28**, 511–515 (2010). doi:10.1038/nbt.1621

63. N. Salomonis, P. J. Dexheimer, L. Omberg, R. Schroll, S. Bush, J. Huo, L. Schriml, S. Ho Sui, M. Keddache, C. Mayhew, S. K. Shanmukhappa, J. Wells, K. Daily, S. Hubler, Y. Wang, E. Zambidis, A. Margolin, W. Hide, A. K. Hatzopoulos, P. Malik, J. A. Cancelas, B. J. Aronow, C. Lutzko, Integrated genomic analysis of diverse induced pluripotent stem cells from the Progenitor Cell Biology Consortium. *Stem Cell Rep.* **7**, 110–125 (2016). doi:10.1016/j.stemcr.2016.05.006

64. B. Langmead, C. Trapnell, M. Pop, S. L. Salzberg, Ultrafast and memory-efficient alignment of short DNA sequences to the human genome. *Genome Biol.* **10**, R25 (2009). doi:10.1186/gb-2009-10-3-r25

65. D. Kim, B. Langmead, S. L. Salzberg, HISAT: A fast spliced aligner with low memory requirements. *Nat. Methods* **12**, 357–360 (2015). doi:10.1038/nmeth.3317

66. Y. Liao, G. K. Smyth, W. Shi, featureCounts: An efficient general purpose program for assigning sequence reads to genomic features. *Bioinformatics* **30**, 923–930 (2013). doi:10.1093/bioinformatics/btt656

67. S. Anders, W. Huber, Differential expression analysis for sequence count data. *Genome Biol.* **11**, R106 (2010). doi:10.1186/gb-2010-11-10-r106

68. H. O'Geen, L. Echipare, P. J. Farnham, Using ChIP-seq technology to generate high-resolution profiles of histone modifications. *Methods Mol. Biol.* **791**, 265–286 (2011). doi:10.1007/978-1-61779-316-5_20

69. B. Langmead, S. L. Salzberg, Fast gapped-read alignment with Bowtie 2. *Nat. Methods* **9**, 357–359 (2012). doi:10.1038/nmeth.1923

70. F. Ramírez, D. P. Ryan, B. Grüning, V. Bhardwaj, F. Kilpert, A. S. Richter, S. Heyne, F. Dündar, T. Manke, deepTools2: A next generation web server for deep-sequencing data analysis. *Nucleic Acids Res.* **44**, W160–W165 (2016). doi:10.1093/nar/gkw257